RV ARAON research activities within US EEZ waters in 2016

1. Research activities

Araon Arctic Cruise (ARA07B) departed Nome, Alaska on August 5, 2016 and returned to Barrow on August 21, 2016. With funding provided by the Ministry of Oceans and Fisheries (MOF) and by Korea Polar Research Institute (KOPRI), the aim of the cruise was to investigate the structure and processes in the water column and subsurface (sediment) around the Bering/Chukchi/Beaufort/East Siberian Seas in rapid transition. The research effort was the conducted research cruise of the Korea-Arctic Ocean Observing System (K-AOOS) Program with support from the MOF and the KOPRI. Total of 43 scientists have participated from 8 countries (Korea, US, China, Japan, U.K., France, Spain, Vietnam) representing 18 different universities and research organizations. Araon data were collected on the physical, biological, chemical, and biogeochemical properties the US EEZ waters (Fig. 1.1).

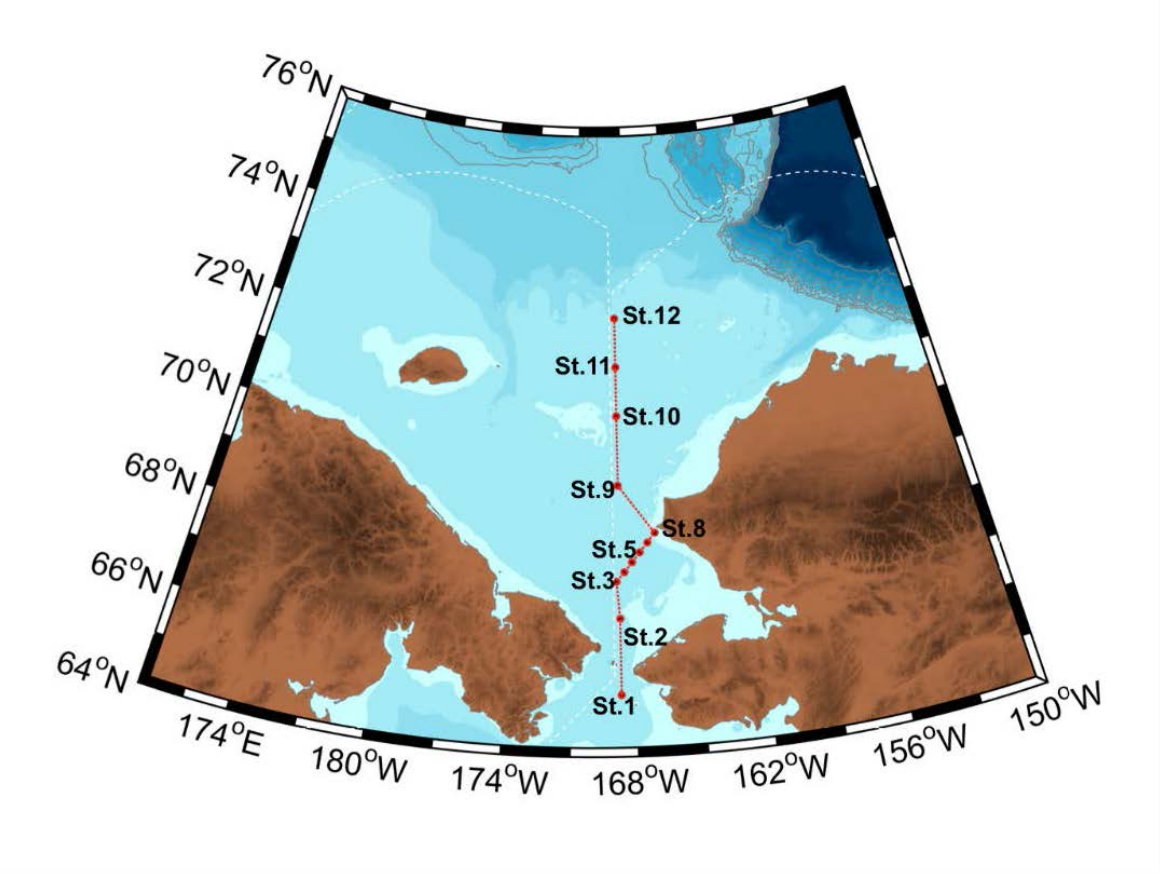

Figure 1.1. A station map of Arctic cruise with color-mapped bathymetry. Red circles are study stations. White dashed lines denote Russian EEZ and US EEZ lines. Work/transit in the US EEZ was performed during 5th

August – 9th August 2016.

2. Research Methods

1) Physical Oceanography

An intensive oceanographic survey with 12 hydrographic stations was conducted in the Chukchi Sea within US EEZ during the period of August 5 to August 8, 2016. Along the transect of hydrographic stations, vertical profiles of temperature, salinity, density, dissolved oxygen, fluorescence, transmissivity and PAR, and water samples were obtained from the hydro-casts of a SBE32 carousel water sampler equipped with a SBE9plus CTD profiler, a SBE43 dissolved oxygen sensor, a transmissometer, PAR and fluorometer, and 24 position rosette with 10-liter Nisken bottles. During the CTD upcasting, water samples were collected at several depths for biochemical analyses. For the precise reading, the salinities of collected water samples were further analyzed by an Autosal salinometer (Guildline, 8400B). The measurement was performed when the temperature of water samples was stabilized to a laboratory temperature, usually within 24-48 h after the collection.

2) Nutrients and dissolved and particulate organic carbon and nitrogen in the Arctic Ocean

Seawater sampling for nutrients (PO_4, NO_2+NO_3, NH_4, and SiO_2), dissolved organic carbon and nitrogen (DOC and DON) and particulate organic carbon and nitrogen (POC and PON) was carried out at 12 stations in the Chukchi Sea using a CTD/rosette sampler holding 24-10 L Niskin bottles (SeaBird Electronics, SBE 911 plus) during Korea research ice breaker R/V Araon cruise (ARA07B, August 6–8, 2016) (Fig. 1.1).

a. Nutrients

Samples for nutrients were collected from the Niskin bottles into 50 ml conical tubes and immediately stored in a refrigerator at 4°C prior to chemical analyses. All nutrients samples were analyzed onboard within 3 days. Concentrations of nutrients were measured using standard colorimetric methods adapted for use on a 4-channel continuous Auto-Analyzer (QuAAtro, Seal Analytical). The channel configurations and reagents were prepared according to the 'QuAAtro Applications'. Standard curves were run with each batch of samples using freshly prepared standards that spanned the range of concentrations in the samples. The r^2 values of all the standard curves were greater than or equal to 0.99. In addition, reference materials for nutrients in seawater (RMNS) provided by 'KANSO Technos' (Lot. No. 'BV') were used along with standards at every batch of run in order to ensure accurate and inter-comparable measurements.

b. Dissolved organic carbon and nitrogen

For DOC and DON measurements, seawater sample was drawn from the Niskin bottle by gravity filtration through an inline pre-combusted (at 550°C for 6 hours) Whatman GF/F filter held in an

acid-cleaned (0.1 M HCl) polycarbonate 47 mm filter holder (PP-47, ADVANTEC). The filter holder was attached directly to the Niskin bottle spigot. The filtrate was collected in an acid-cleaned glass bottle and then distributed into two pre-combusted 20 ml glass ampoules with a sterilized serological pipette. Each ampoule was sealed with a torch, quick-frozen, and preserved at –24°C until the analysis in our land laboratory. Analyses of DOC and DON were performed by high temperature combustion using a Shimadzu TOC-L analyzer equipped with an inline chemiluminescence nitrogen detector (Shimadzu TNM-L). Milli-Q water (blank) and consensus reference material (CRM, 42–45 μM C, deep Florida Strait water obtained from University of Miami) were measured every sixth analysis to check the accuracy of the measurements. The precision of the DOC measurements was 2–3 μM or a CV of 3–5%.

c. Particulate organic carbon and nitrogen

For determination of POC and PON, seawater sample was drawn from the Niskin bottle into an amber polyethylene bottle. Known volumes (2 L) of seawater were filtered onto pre-combusted Whatman GF/F filters (25 mm) using a filtering system under gentle vacuum at < 0.1 MPa. To prevent data scattering, large zooplankton (e.g., copepods) were removed from the filter samples using tweezers after washing with filtered seawater if they were captured on the filters. These filter samples were stored at –80°C until the analysis in our land laboratory. Before POC analyses, the filter samples were freeze-dried, and then exposed to HCl fumes for 24 h in a desiccator to remove inorganic carbon from the samples. Measurements were carried out with a CHN elemental analyzer (vario MACRO cube, Elementar, Germany). Acetanilide was used as a standard. The precision of these measurements was ± 1.0 μmol L^{-1}.

3) Dimethylsulfide (DMS) and dimethylsulphoniopropionate (DMSP)

Seawater samples with CTD sampling were taken for gas chromatographic (GC) measurements of DMS. Seawater was filtered on a Whatman 40-mm GF/F filter and poured into a glass vial bottle for DMS measurement, although dissolved DMSP (DMSPd) and particulate DMSP (DMSPp) samples were not filtered. DMS was measured by a GC-flame photometric detector (FPD) (GC-2014, Shimadzu) with an automatic purge & trap extraction/pre-concentration system as soon as possible after sampling. Briefly, seawater sample was introduced into a purge bottle and extracted by pure N_2 carrier gas for 14 minutes. Extracted gas stream including DMS passed through cold dehydration trap (dry ice/ethanol cooled hollow U-shaped glass tube) and concentrated on the cold trap (dry ice/ethanol temperature) with TENAX TA. Concentrated gas was eliminated by replacing the Dewar bottle of from dry ice/ethanol refrigerant to boiled water. Eliminated gas was introduced to GC-FPD. After sampling, sample for DMSPd was gravity filtered by Whatman 40-mm GF/F filter and 4-mL of filtered seawater was collected as a subsample. 8-mL of seawater sample

was taken as DMSPp subsample. We added 0.2- and 0.4-mL of HCl solution for preservation for DMSPd and DMSPp samples, respectively.

4) UV absorbing compound (Mycosporine-like amino acids; MAAs) and light intensity in the Arctic Ocean

The study station was location in the western Arctic Ocean (Chukchi Sea and East Siberian Sea) in August 2016, during the cruise of R/V ARAON. The seawater samples were determined from CTD casts made using a Sea-Bird 911 plus system (Sea-Bird, Inc., NY, USA). Hydrocasting of the CTD/Rosette system was conducted to measure the profiles of temperature, salinity, and depth.

a. UV absorbing compound (Mycosporine-like amino acids)

MAAs were extracted according to Sinha et al. (2001) and Ha et al. (2012). To analyze the MAA contents in the samples, 4 L of each sample was filtered through pre-combusted (450℃, 4 h) glass fiber filters (47 mm) and stored at -80℃ until analysis. A 3 mL volume of 100 % MeOH was then added to the samples, and an ultrasonicator (30 s, 50 W; Ulsso Hi-tech ULH-700s) was used to disrupt them. The samples were next placed in a freezer at 4 ℃ overnight, after which the solvent phase was transferred to a 2 mL microtube through a 0.2 μm syringe filter (PTFE 0.2 μm Hydrophobic). A centrifugal evaporator (CVE-200D, EYELA, Japan) was employed to completely dry the solvent. The dried sample was then dissolved in 500 μL of distilled water, and 100 μL of chloroform was added to remove lipids and pigment. The sample was subsequently centrifuged for 10 min at 10,000 rpm. A 400 μL aliquot of the supernatant was finally separated and injected into a high-performance liquid chromatograph (HPLC) (Agilent Technologies 1200 series, USA) to quantitatively analyze the MAA contents.

b. Light intensity

To estimate the penetration of UV-B, UV-A, and PAR in the water column, radiation were measured by RMSES radiometer (TriOS GmbH, Germany) at each sampling stations. We measured the radiation from surface to 40 m the UV-B (280 nm – 320 nm), UV-A (320 nm-360 nm), and PAR (400 nm – 700 nm) as the intensity (W/m^{-2})

5) Estimation of Nitrogen source using CSIA-AAs

Nitrogen isotope analysis for background nitrogen in Arctic waters was performed using zooplankton, Calanus spp. (Fig. 2.5.1). The zooplankton samples were collected by using 500 μm net, and stored in deep freezer(-80 ° C). The samples were transferred to the laboratory and

lyophilized. The lyophilized zooplankton samples were homogenized to analyze amino acids and bulk nitrogen isotopes.

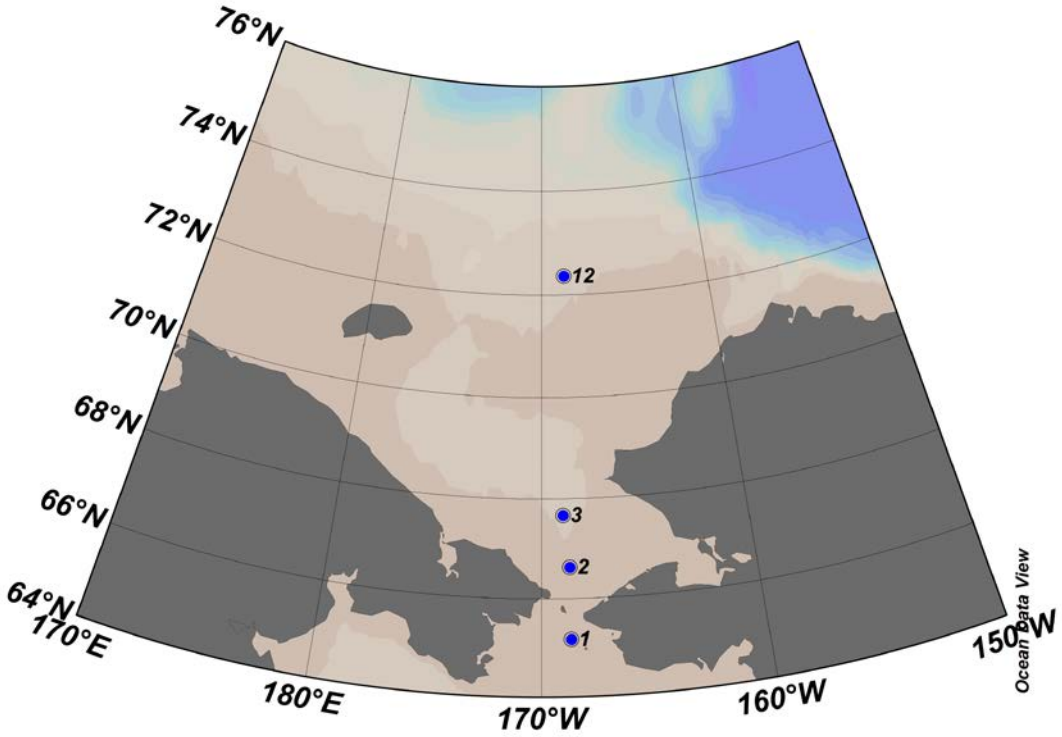

Figure 2.5.1. Map of sampling stations (black dots) with sampling station number

Bulk nitrogen stable isotope ratio of zooplankton was analyzed using a stable isotope mass spectrometer (EA-IRMS) interlocked with an elemental analyzer. As a oxidation column of EA, quartz tube filled with Chromium oxide and Cobalt oxide was used at 1020°C, and as a reduction column, quartz tube filled with Copper was used at 650°C. During the analysis of each samples, we determined the degree of accuracy through performing repetitive analyze of N-1(0.4‰, IAEA).

The nitrogen stable isotope ratio of zooplankton amino acid was analyzed using GC-IRMS, which is isotope ratio mass spectrometer interlocked with gas chromatography, after hydrolysis, lipid removal, derivatization. As a oxidation column of GC-IRMS, quartz tube filled with copper oxide, nickel oxide and platinum wire was used at 950°C, and as a reduction column, ceramic tube filled with copper and rhodium wire was used at 650°C. GC column, which is for separating each amino acid compounds, was HP-ultra-2(Agilent, USA). The flow rate was 1.0ml/min during analyze. The standard deviation of reference gas stability in the IRMS was less than 0.1‰, and we confirmed precision through analyzing standard after analyzing each three samples.

The sea water samples were collected in station 1, 3 and 12 (3~4 depth of each station) for analysis stable oxygen isotope ratio, which could be calculated to water-mass fraction. Samples were filtered by PTFE filter (Advantec, 0.2μm) and stored in 2ml GC vial at 4°C until analysis. The

stable oxygen isotope ratio of seawater analyzed by IRMS(Isotope Ratio Mass Spectrometer, Isoprime 100, Isoprime, U.K) interlocked with Elemental Analyzer (Pyrogenic EA, Elementar, U.K). During the analysis of each samples, we determined the degree of accuracy through performing repetitive analysis of V-SMOW (0±0.02‰, IAEA).

6) Air-sea CO_2 exchange and water column carbonate system

a. Air-sea CO_2 flux

CO_2 flux across the sea surface is usually determined by the concentration difference between the dissolved CO_2 in the surface mixed layer and the atmospheric CO_2 overlying the surface with a parameterized gas transfer velocity k. Dissolved CO_2, so called pCO_2, was determined using an aqueous and gaseous phase equilibration technique with a small Weiss-type equilibrator. The air above the surface was withdrawn from the intake cup mounted at the foremast at 29 m above sea-level. The CO_2 in the air and the equilibrator headspace was analyzed with Li-cor 7000 in which 4.5 um wavelength of photon is selectively absorbed by CO_2. The analyzing system was calibrated every 6 hours using a series of calibration gases and one zero air. pCO_2 in the seawater was acquired every minute in a computer and atmospheric CO_2 every 6 hours. The raw data was corrected for the effect of temperature difference between the in-situ and the equilibrator after coming back to the institute, and gas transfer velocity was determined using parameterization with wind speed which has been logged in DADIS onboard Araon.

b. Carbonate system of the water column

Carbonate system in the water column compose of ionic form of carbonate (CO_3^{2-}), bicarbonate (HCO_3^-), hydrogen ion (hydronium) and neutral form of carbonic acid and dissolved CO_2. These carbonate species exist in equilibrium in seawater depending on alkalinity of the seawater. These species, however, cannot be analyzed directly using analytical instruments except CO_2 and hydronium. Thus, to determine the carbonate system in the water column, we measure total dissolved inorganic carbon (DIC) and total alkalinity (TA) by which one can derive ionic and neutral form of carbonate system. DIC and TA are defined as follows:

$$DIC = [HCO_3^-] + [CO_3^{2-}] + [CO_2] + [H_2CO_3]$$

$$TA = [HCO_3^-] + 2[CO_3^{2-}] + \Sigma[anions] - \Sigma[cations]$$

DIC and TA were analyzed in the laboratory after collecting seawater samples aboard at the hydrographic stations. To prevent the seawater samples from being altered due to biological activities in the seawater, 100 uL of $HgCl_2$ solution (50%) were injected upon collecting the samples from the Niskin seawater collected attached in CTD/Rosette. The sample bottles were flushed 3

times before starting collection in 250 mL bottle. Making small headspace, injecting $HgCl_2$ solution, and tightening the lid with black electric tape, the samples were stored in a dark place before analysis.

We also collect seawater samples for analysis of pH onboard. The procedure of collection is the same as that for DIC and TA.

To analyze dissolved CO_2 in the water column, a specially designed bottle was employed to avoid contact with ambient air onboard. The bottle composes of one stopcock and septum lid on both sides. Seawater flows through these two ends and the body of the bottle which was upright overflowing a certain time period to flush the bottle and to get rid of any bubbles inside. Upon collecting the seawater, 50 mL of CO_2 free N_2 gas was injected into the jar to equilibrate it with the water in. The equilibrated headspace air was then analyzed onboard or in the laboratory. 40 uL of $HgCl_2$ was injected to avoid contamination from biological activities.

7) Microbial Oceanography

During the Araon cruise in 2016, prokaryotic (i.e. Bacteria and Archaea) and viral abundances were measured at stations 1, 3, 10 and 12 within US EEZ waters. In addition, environmental genomic DNAs of prokaryotes and viruses were obtained and preserved as archives for future study. Sampling and analysis methods are shown in detail in the following.

Seawater sampling for microbiological study was made at 4 stations. Samples were collected from 2-3 depths (surface to ca. 40 m) with 10 L Niskin bottles mounted on a CTD rosette. For measurements of viral and prokaryotic abundances, seawater samples (10 ml) were fixed with 0.02 μm filtered formalin (final conc. of 2%), and were stored at -80°C.

Seawaters (1-2 L) for collecting genomic DNAs of prokaryotes were pre-filtered through 3.0 μm pore-sized Nuclepore filters (Whatman) and concentrated onto 0.2 μm pore-sized Nuclepore filters (Whatman). Filters were immediately transferred to cryovial tubes and stored at -80°C. In a land-based laboratory, extraction of nucleic acids was made as previously described by Bowman et al. (2012).

References

Bowman, J. S., Rasmussen, S., Blom, N., Deming, J. W., Rysgaard, S., and Sicheritz-Ponten, T. (2012) Microbial community structure of Arctic multiyear sea ice and surface seawater by 454 sequencing of the 16S RNA gene, The ISME Journal, 6, 11-20

8) Chlorophyll-a concentrations and photosynthetic pigments

The photosynthetic pigments and chlorophyll-a data were collected in the Chukchi Sea in 2016. A total of 12 stations were visited. Water samples were collected at 4-6 depths (Surface, 10m, 20m, 30m, 50m, and subsurface chlorophyll-a maximum depth) with a rosette sampler equipped with 10 L Niskin-type bottles, an in situ fluorometer, and a high-precision Sea-Bird plus CTD probe.

Subsamples from the Niskin bottles were filtered through a cascade connection of 20-μm nylon mesh, Nuclepore filter (Whatman International) with pore size of 2 μm, and a Whatman GF/F filter to determine size-fractionated chlorophyll-a concentrations. Thus, micro (>20 μm), nano (2-20 μm), and pico-sized (<2 μm) chlorophyll-a concentrations could be measured directly. Subsamples for total chlorophyll-a were filtered onto 47 mm GF/F Whatman filters. Each filter was extracted in 90% acetone for 24 hours at 4 ºC in darkness, and chlorophyll-a concentrations were measured with a fluorometer (model Trilogy, Turner Designs, USA; method: Parson et al., 1984).

For photosynthetic pigments' analysis, 2 – 4 L seawater samples of surface and SCM layers were filtered onto 47 mm GF/F Whatman filters and stored at －80 °C. The filters were extracted with 3 mL 100 % acetone, ultrasonicated for 30 sec and maintained under 4 °C in dark for 15 hours. Debris was removed by filtering through 0.45 μm Teflon syringe filters. Just before injection, the extracts were diluted with distilled water to avoid the peak distortion of the first eluting pigments. Pigments were assessed by HPLC (Agilent series 1200 chromatographic system, Germany) with C8 column (Agilent XDB-C8, USA) following the method of Zapata et al. (2000).

9) Phytoplankton communities composition

The data were collected in the Bering Strait and Chukchi Sea from August 5 to 9 in 2016. A total of 12 stations were visited. Water samples were collected at 4-6 depths (Surface, 10m, 20m, 30m, 50m, 100m, and subsurface chlorophyll a maximum depth) with a rosette sampler equipped with 20 L Niskin-type bottles, an in situ fluorometer, and a high-precision Sea-Bird plus CTD probe. The subsurface chlorophyll maximum layer depths were estimated by CTD profiles. To analysis phytoplankton community composition, water samples were obtained with a CTD/rosette unit in 20 L PVC Niskin bottles during the 'up' casts. Aliquots of 125 mL were preserved with glutaraldehyde (final concentration 1%). Sample volumes of 50 to 100 mL were filtered through Gelman GN-6 Metricel filters (0.45 μm pore size, 25 mm diameter). The filters were mounted on microscopic slides in a water-soluble embedding medium (HPMA, 2-hydroxypropyl methacrylate) on board. The HPMA slides were used for identification and estimation of cell concentration and biovolume. The HPMA-mounting technique has some advantages over the classical Utermöhl sedimentation method.

Samples were also collected via phytoplankton net tows (20 μm mesh) and preserved with glutaraldehyde (final concentration 2%); these samples were used only for identification of small species in the phytoplankton assemblage. Since the results from this can be biased towards larger specimens, these data were not used for statistical analysis, but only for morphological and systematic analysis.

10) Primary production and macromolecular composition

ARAON Arctic Cruise (ARA07B) in the US EEZ was conducted from August 5 to 8, 2016. The Arctic environment is changing rapidly due to global warming and anthropogenic activities. In particular, phytoplankton as the primary producer is sensitive to changes in the marine conditions, which can affect higher trophic levels. Therefore, studies on the primary productivity and biochemical composition of phytoplankton are needed to understand present status and predict the future of marine ecosystems in the Arctic.

First, water samples were obtained from six light depths (100, 50, 30, 12, 5, and 1 %) using a CTD rosette sampler. To estimate carbon and nitrogen uptake rates of phytoplankton, stable isotope reagents (^{13}C, $^{15}NO_3$, $^{15}NH_4$) were added to each bottle and then incubated for 4-5 hours on the deck under the natural light. After incubation, samples were filtered through GF/F (Whatman, 0.7 μm pore, ø = 25 mm) filter paper and stored at -80 °C until analysis. Both carbon and nitrogen isotope abundances were determined by a IRMS (Isotope-ratio mass spectrometer) after the carbonate removal. For background data, water samples were collected alkalinities and major nutrient concentrations (nitrate, nitrite, and ammonium).

Second, water samples for macromolecular composition of phytoplankton obtained from 3 light depths (100, 30, and 1%). Each seawater sample went through a 47 mm GF/F filter (Whatman, 0.7 μm pore) and was then immediately stored at -80 °C prior to biochemical analysis. The content of carbohydrates was determined by phenol-sulfuric method from Dubois et al. (1956) and particulate protein content was determined by the Lowry method (1951). For lipid extraction and assay from 1:2 (v/v) chloroform-methanol mixture and tripalmitin solutions were used (Bligh and Dyer, 1959; Marsh and Weinstein, 1966). The three particulate organic extracts from a blank GF/F filter were used as controls.

11) Protozoa abundance and grazing rates on phytoplankton

To determine the abundance and composition of heterotrophic protists, a CTD-Niskin rosette sampler was used to take water samples from the following 4-5 depths. For ciliates, 500 ml water from the vertical profiles was preserved with 1% acid Lugol's iodine solution these samples were

then stored in darkness. For heterotrophic nanoflagellates and heterotrophic dinoflagellates smaller than 20 μm, 200 ml of water was preserved with glutaraldehyde (0.5% final concentration) and it was made with slide to analyze microscope. Grazing rates of heterotrophic protists on phytoplankton were determined by the dilution method (Landry and Hassett 1982). Water for grazing experiments was collected from 2 depths (surface, SCM) of each station, and gently filtered through a 200-μm mesh. At each station, 30L seawater were collected in a Niskin bottle and transferred to a polycarbonate carboy. Part of this water was filtered through the 0.22-μm filtration system. Dilution series were set up in ten 1.3-l PC bottles. Ten bottles were used to establish a nutrient-enriched dilution series consisting of replicate bottles with 20 and 100% natural seawater. The bottles were incubated on deck for 24-48h at ambient sea surface temperatures and screened to the ambient light level with neutral density screening. Subsamples were collected from replicate bottles at 0 and 24-48h to determine chlorophyll-a concentrations.

12) Mesozooplankton abundance and composition

To estimate the abundance of zooplankton and its compositions, net samples were collected with a Bongo net (60 cm diameter, 330 and 500 μm mesh) at 9 selected stations The net was towed vertically within the upper 200 m of the water column for about 10 – 15 min. The filtering of seawater for each sample was indicated by revolution counts of a flow meter attached to the net. The half of samples from 330 μm net was immediately fixed and preserved with 10% neutralized formaldehyde for quantitative analyses. Subsampling will carried out using a Folsom plankton splitter, and abundance will be expressed in terms of individual numbers per cubic meter using volume filtered by net, obtained from the revolution counts of a flow meter attached to the net. Subsamples from 500 μm net were transferred to 20-ml vials with natural seawater, which were frozen at –80 °C for the post analysis.

13) Phytoplankton physiology (photochemistry)

To investigate the impact of physico-chemical conditions on photosynthesis in the study area, we measured photosynthetic characteristics of phytoplankton at total 7 stations (including three DBO stations) using a Fluorescence Induction and Relaxation (FIRe) system (Fig. 2.13.1). Continuous measurements also conducted on underway (using pumped on seawater around 7 m depth beneath the ship) during the Araon transit. Active fluorometry is a non-destructive and rapid method, and it has been used to monitor variations in the photochemistry (Kolber and Falkowski, 1993; Falkowski and Kolber, 1995). These measurements provide an express diagnostics of the effects of environmental factors on photosynthetic processes such as nutrient limitation. After collection from Niskin bottles at 5 - 6 depths within 100 m, samples were kept under in situ temperature in light

bottles. These samples were measured after 30 minutes low light adaptation. Photosystem II (PSII) parameters such as the minimal fluorescence yield (F0; when all reaction centers are open), the maximal fluorescence yield (Fm; all reaction centers are closed), the quantum efficiency of PSII (Fv/Fm), the functional (or effective) absorption cross-section of PSII (σPSII) were measured as describe in Kolber et al. (1998). Quantum efficiency of photochemistry in PSII (Fv/Fm) was calculated as a ratio of variable fluorescence (Fv=Fm-F0) to the maximum one (Fm). The fluorescence measurements were corrected for the blank signal recorded from filtered seawater (by 0.2 um syringe filter set). When the ship was underway pumped on the seawater near surface and the fluorescence was measured continuously on real time.

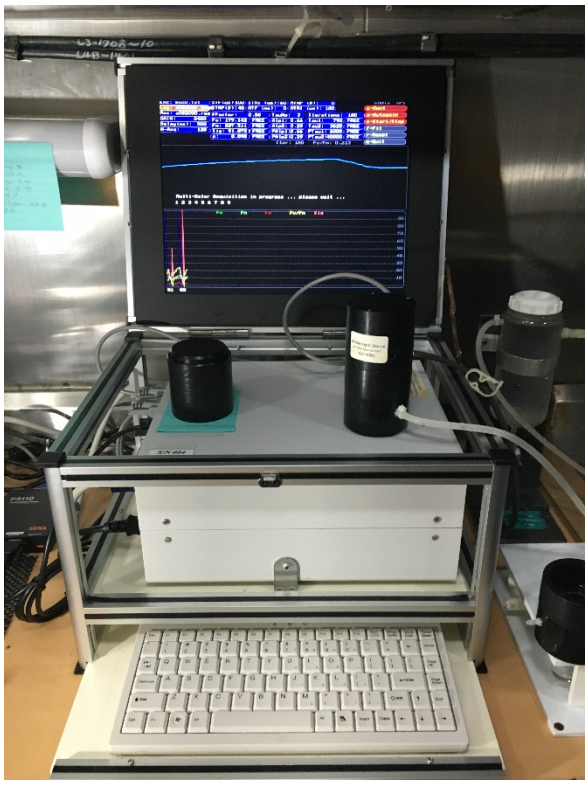

Figure 2.13.1. A custom-built Fluorescence Induction and Relaxation (FIRe) system onboard Araon

14) Ocean Optical Observation

In this cruise, we tried to obtain bio-optical relationships to improve ocean color data quality by observing absorptions from phytoplankton, suspended sediment (SS), inherent optical properties (IOPs) of water (e.g. absorptions by colored dissolved organic matters (CDOM)) and apparent optical properties (AOPs) of water (e.g. downwelling irradiances (Ed) and upwelling radiance (Lu)). Our major goal in this study was to collect bio-optical data in conjunction with measurements of CDOM, phytoplankton and SS absorption in support of NASA's efforts to develop robust empirical and semi-analytic algorithms for ocean color products in high latitude regions. This effort is a part of longer strategic objective of understanding the impacts of changing climate on biological

oceanographic processes in the Arctic Ocean using ocean color satellite data.

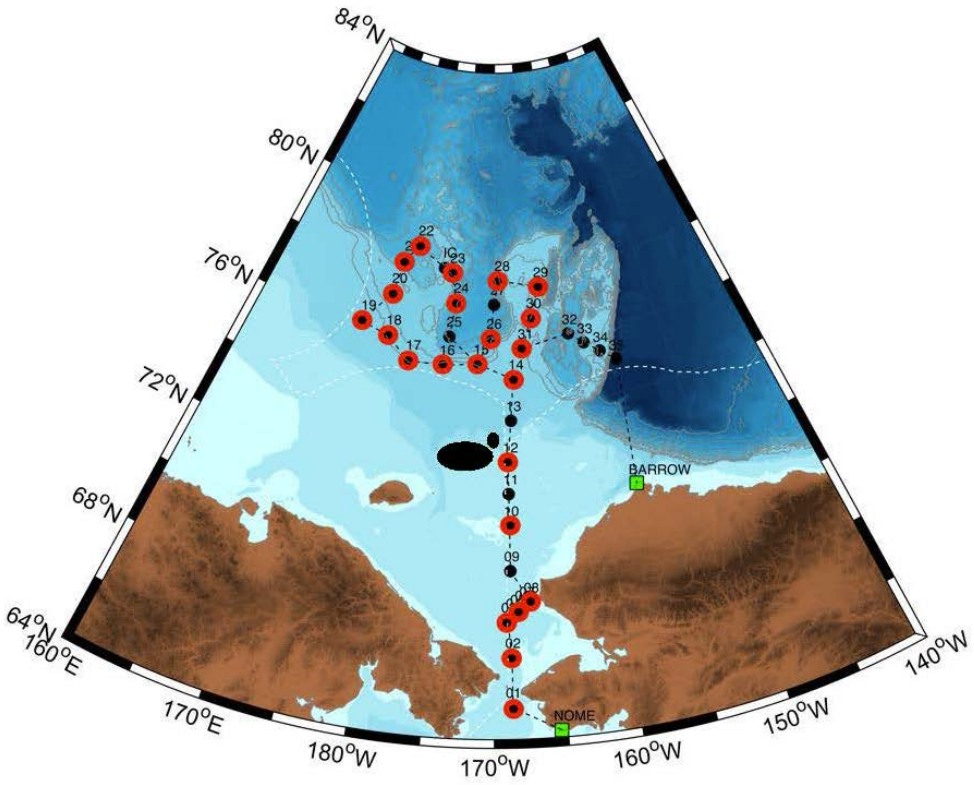

Figure. 2.14.1. A station map for ocean optical observation (red dot : station, black dot : underway water sampling point).

We sampled 69 waters at 23 stations (with 3 depths of surface, subsurface chlorophyll maximum, and bottom within euphotic depth) and 23 intermediate sites between stations in underway route (Fig. 2.14.1). To measure inherent optical properties (IOPs) of water, seawater volumes of 500 - 2,000 ml were filtered on 25 mm glass-fiber filters. Optical densities of total particulate matters were measured directly on the wet filters by methods of Truper and Yentch (1967) with a double-beam recording spectrophotometer (Cary100, Agilent Technologies) in a spectral range 250 - 800 nm (spectrum resolution of 1 nm). The filter was placed in front of diffusing windows adjacent to an end-on photomultiplier of large surface area. For a reference blank and baseline variations, an unused wetted filter was used, and the instrument was taken as were automatically corrected. After the measurement of optical density of total pigments, the spectral absorption by non-algal material was measured separately with the method of Kishino et al. (1985).

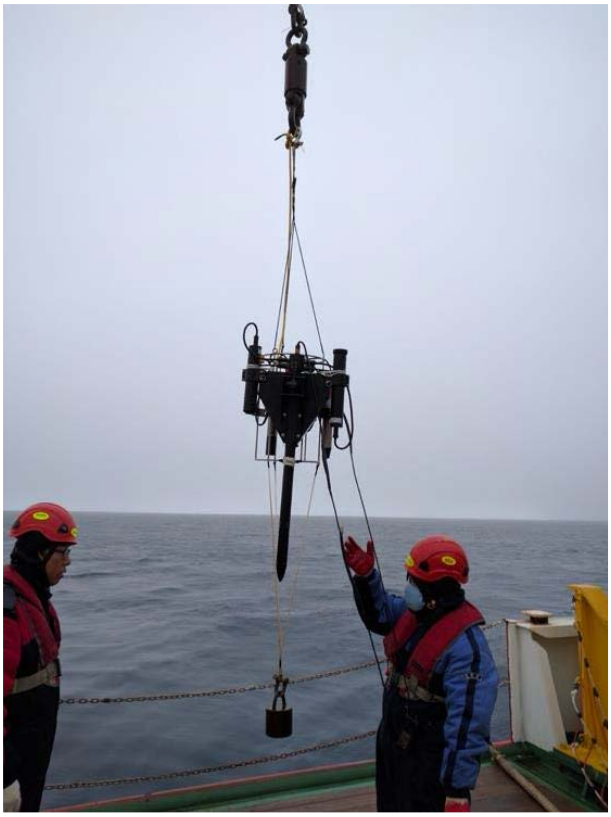

Figure. 2.14.2. Deploy of hyper-spectrometer (HPRO II and TriOS).

For the measuring apparent optical properties (AOPs) of water, we deployed hyper-spectrometer (HPRO II and TriOS, Fig. 2.14.2) with a spectral range of 350 - 800 nm (HPRO II), 280 - 950 nm (TriOS) of downwelling irradiance (Ed) and upwelling radiance (Lu). For the reference as ambient irradiance variation, downwelling irradiance (Es) was measured on deck in a place without shade. The integrated instruments deployed through the A-frame at the stern of the vessel. The deploying speed was 10 m/min. This data will be able to be used for calibrations and validations of currently operating ocean color remote sensing data.

15) Atmospheric Observations

Atmospheric observations on IBRV Araon include the basic surface meteorological parameters (e.g., air temperature, humidity, pressure and wind) and atmospheric radiative fluxes. All the observations were almost continuous during the cruise, so we obtained various time series along the cruise track. However, CO_2 concentrations were not observed because the eddy-covariance system was not loaded on the ship.

Air temperature and relative humidity are measured by HMP155(Vaisala, Finland); air pressure is measured by PTB110 (Vaisala); and horizontal winds are measured either by propeller-type

anemometer (RM Young, U.S.A.) or 2D sonic anemometer (RM Young). Downwelling shortwave and longwave radiative fluxes are measured by radiometers installed at both foremast and radrmast. All the data are logged at 10-min intervals.

3. Scientific achievements

1) Physical Oceanography

a. Vertical Structures

Vertical structures of potential temperature and salinity at the transection from St. 1 to St. 12 are shown in Figs. 3.1.1 and 3.1.2 (other parameters are plotted in Figs. 3.1.3, 3.1.4, and 3.1.5). The Pacific Water around the Bering Strait (St. 1) is specified with 0-9 °C and 31.0-32.5 psu. Temperature difference between bottom and surface is nearly 9 °C at St. 1. At St. 3, the cold water seems to inflow from the west and prevent the warm water to be extended from the Alaskan coast. At St. 4, relatively warm and fresh water inflows from the west. It appears that the Alaskan Coastal Water (warm and fresh) inflowing along the coast via Bering Strait makes clockwise eddy and then re-flows toward the east (coast). From St. 9 to St. 11, relatively warm water exists on the upper layer (6~8 ^{o}C). As sea ice still exists on the high latitude from St. 12 (Fig. 3.1.5), surface water represents low temperature (< 2 ^{o}C) and relatively fresh (~27 psu).

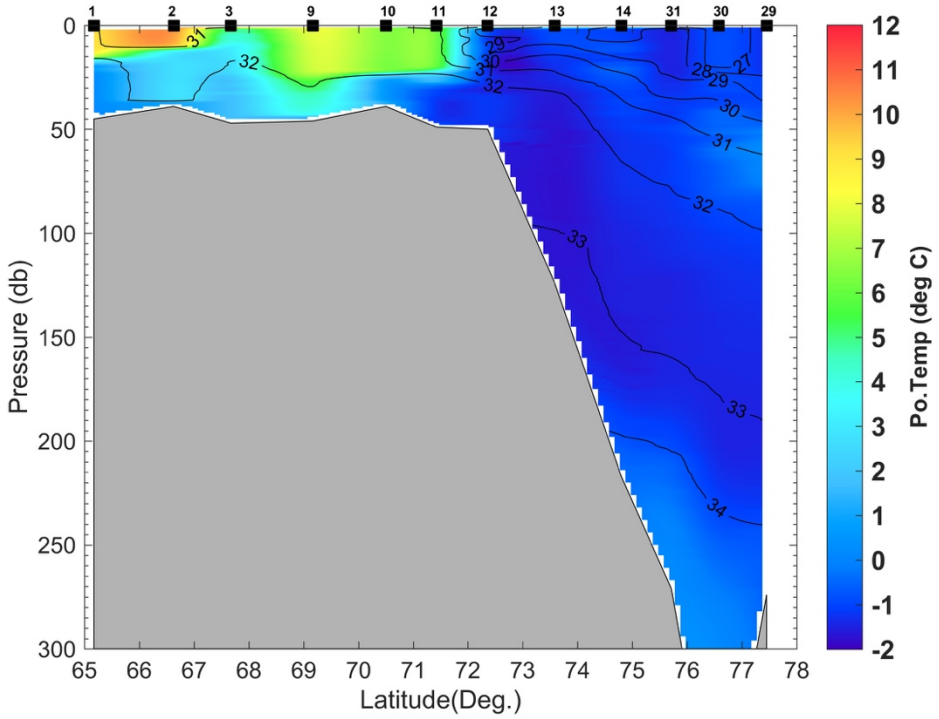

Figure. 3.1.1. Vertical structures of potential temperature and salinity at the transection from St.1 to St.12.

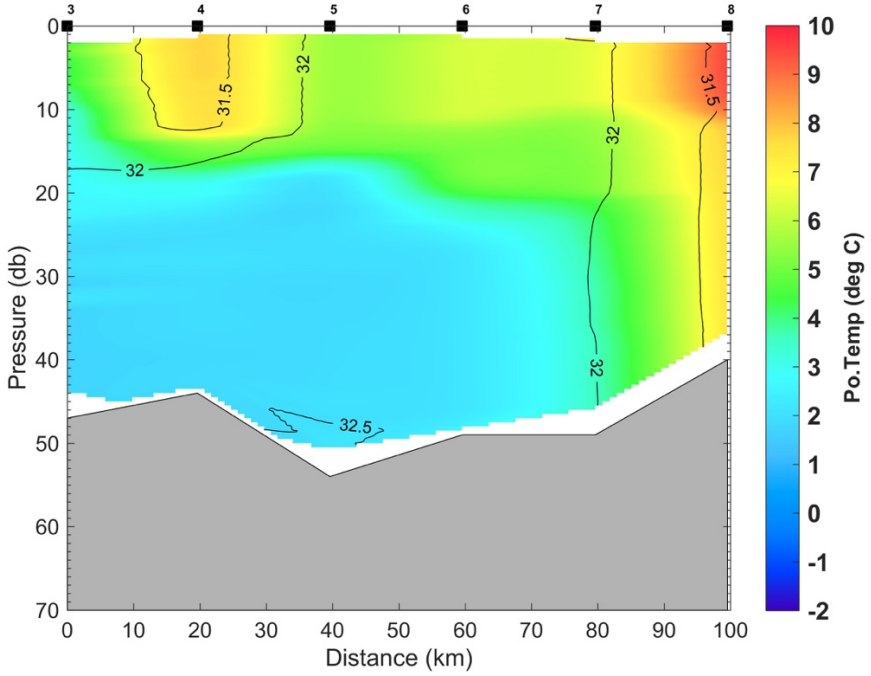

Figure. 3.1.2 Vertical structures of potential temperature and salinity at the transection from St.3 to St.8.

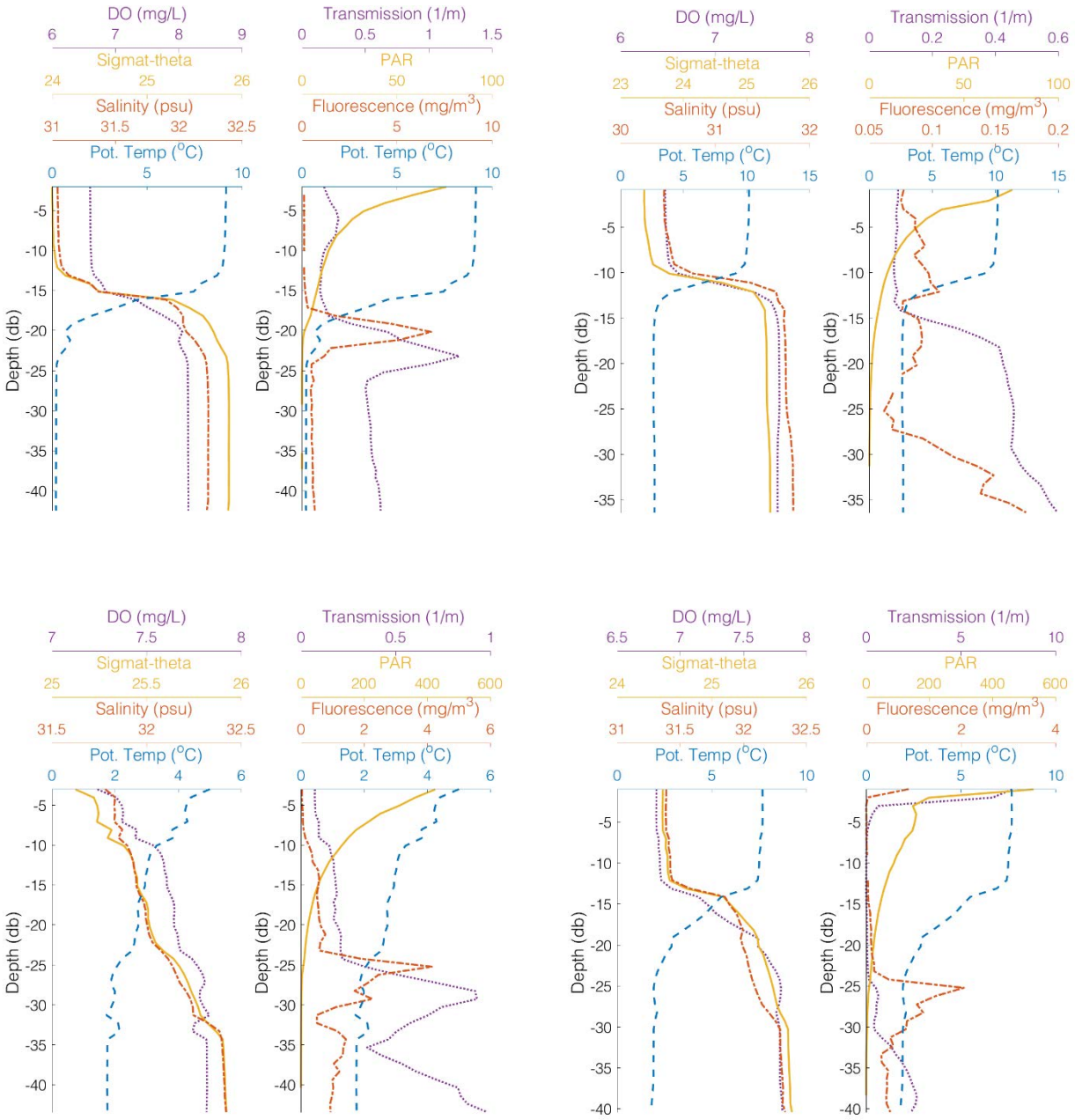

Figure. 3.1.3 Vertical structures of oceanographic parameters (potential temperature, salinity, density, dissolved oxygen, fluorescence, PAR, and transmission) from St.1 to St.4.

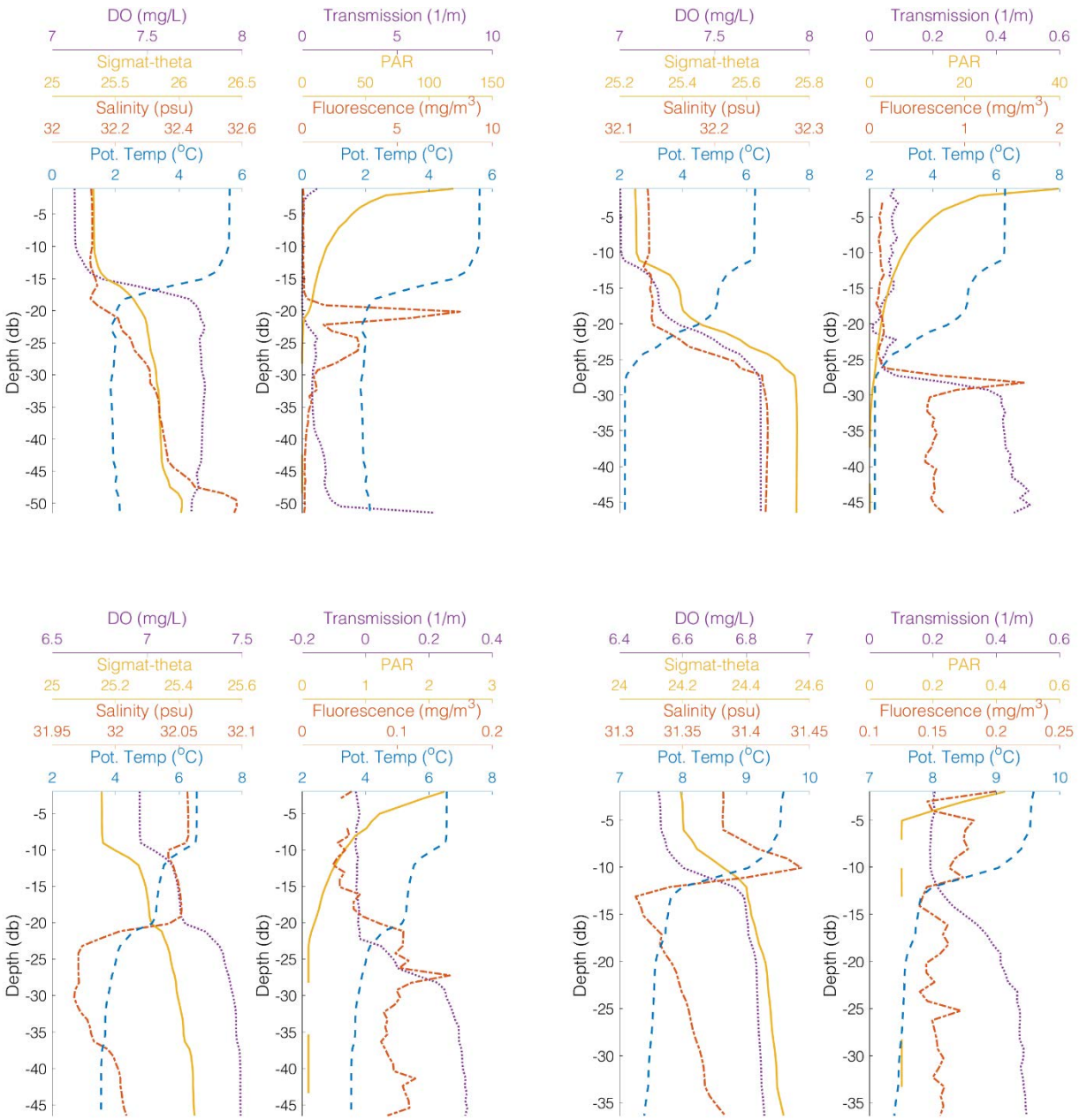

Figure. 3.1.4. Vertical structures of oceanographic parameters (potential temperature, salinity, density, dissolved oxygen, fluorescence, PAR, and transmission) from St.5 to St.8.

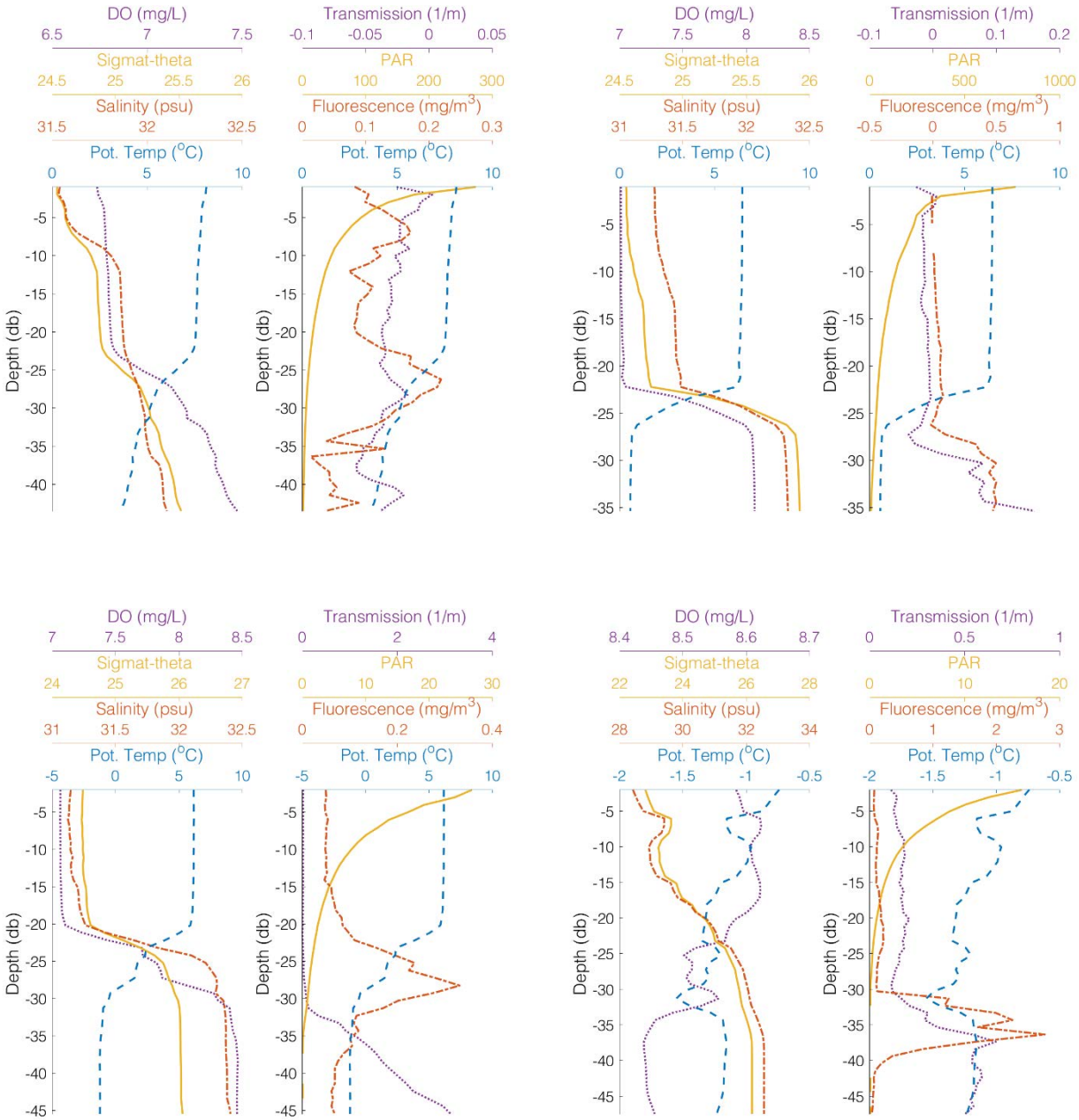

Figure. 3.1.5. Vertical structures of oceanographic parameters (potential temperature, salinity, density, dissolved oxygen, fluorescence, PAR, and transmission) from St.9 to St.12.

2) Nutrients and dissolved and particulate organic carbon and nitrogen in the Arctic Ocean

There was an east–west gradient in water-mass properties across stations 3–8, with the highest nutrient concentrations, highest salinities, lowest temperatures generally occurring in the Anadyr Water in the west; and the lowest nutrient values, and lowest salinities and highest temperature tending to occur in Alaska Coastal Water in the east (Fig. 3.2.1). PO_4 concentration varied from

0.25-0.75 μmol/L in the east side where the influence of Alaska Coastal Water is strong, whereas NO_2+NO_3 concentration was below detection limit, suggesting that primary production in the Arctic Ocean is limited by nitrogen. In contrast, nutrients concentration in the west, where the influence of Anadyr Water is strong, was high. Especially, NH_4 concentration varied from 0.5~5.5 μmol/L, which is derived from the decomposition of particulate organic matter, suggesting active decomposition of particulate organic matter by bacteria in the continental shelf.

For dissolved organic matters, the highest DOC concentration was observed in the eastern side where the influence of Alaska Coastal Water was strong, suggesting that DOC was mainly derived from terrestrial sources. DON showed somewhat different distribution to that of DOC. The distributions of POC and PON were quite similar to that of chlorophyll a concentration. Moreover, the lowest concentrations of POC and PON were found in the eastern side, showing that Alaska Coastal Water is not a significant source of POC and PON, and that POC and PON were derived from marine biological activities.

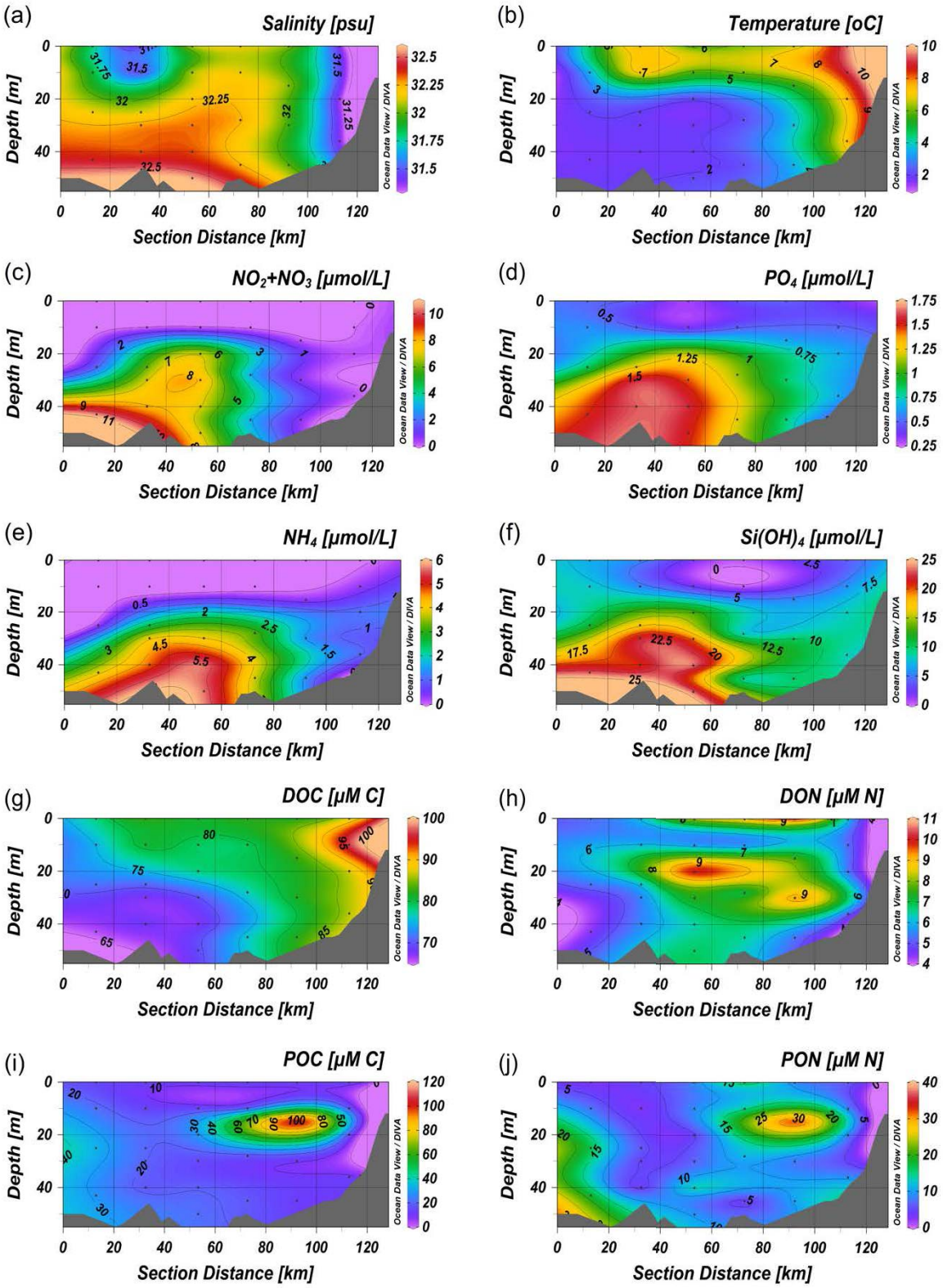

Figure 3.2.1. Salinity (a), temperature (b), PO_4 (c), NO_2+NO_3 (d), NH_4 (e), SiO_2 (f), DOC (g), DON (h), POC (i) and PON (j) concentrations in a section taken from stations 3–8 during the ARA07B cruise.

3) Dimethylsulfide (DMS) and dimethylsulphoniopropionate (DMSP)

Figure 3.3.1 shows distributions of dimethyl sulfide (DMS) dissolved in seawater. The data of station 1 (Bering Strait) was lacked because of a mistake in measurement procedure. There are general trends which shows the maximum in the surface and decrease with the depth except for stations 3 and 4. This general trend means DMS production from biological activities enhanced in the ocean surface. Especially, the DMS concentrations in surface seawater are higher than the other stations from station 2 to station 5, that is, relatively low latitude stations. This result shows the high productivity those stations. We found obvious increase in DMS concentration near sea floor in stations 3 and 4, indicating that there is a source of DMS from the sediment. Considerable factor is that the degradation of organic matter released DMSP and the DMSP was converted to DMS in the sediment. The later stations show the low concentration in DMS (< 1nmol/L) even in the surface. Reduction of biological activation due to low temperature or freshening by sea ice melting may be the factors to make this low concentration in this area. We need to compare the trend to biological parameters such as bacterial activation to clarify the controlling factors.

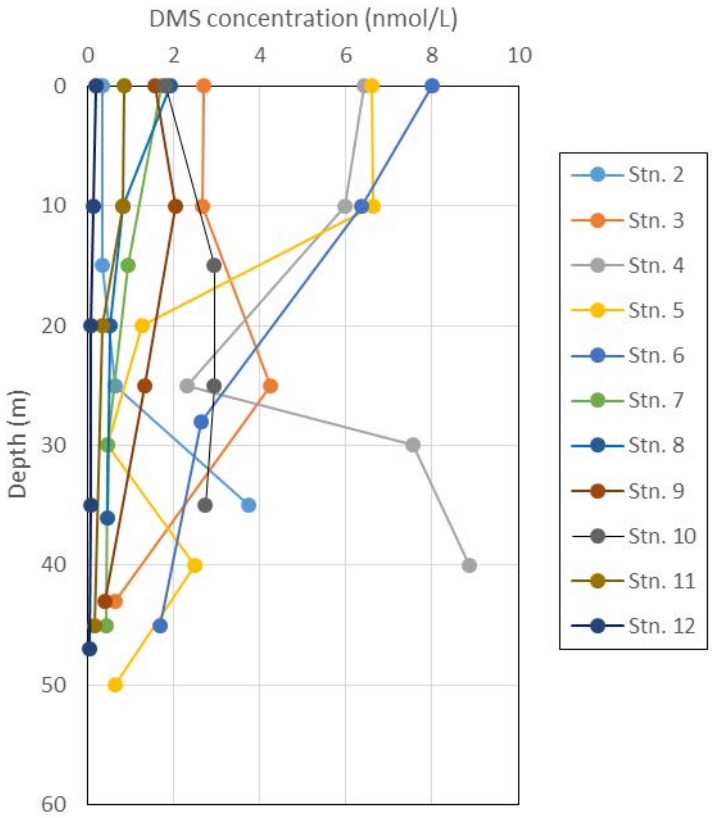

Figure 3.3.1. Vertical profile of DMS measured at stations 2-12 during ARA07B cruise.

4) UV absorbing compound (Mycosporine-like amino acids; MAAs) and light intensity in the Arctic Ocean

a. UV absorbing compound (Mycosporine-like amino acids) MAAs

The total UV absorbing compound (Mycosporine-like amino acids; MAAs) concentration showed the entire study sites with the range from 1.1 to 7.7 ug l^{-1} (fig. 3.4.1). The mean total MAAs concentrations were 3.6 (± 1.9) ug l^{-1} in the study area.

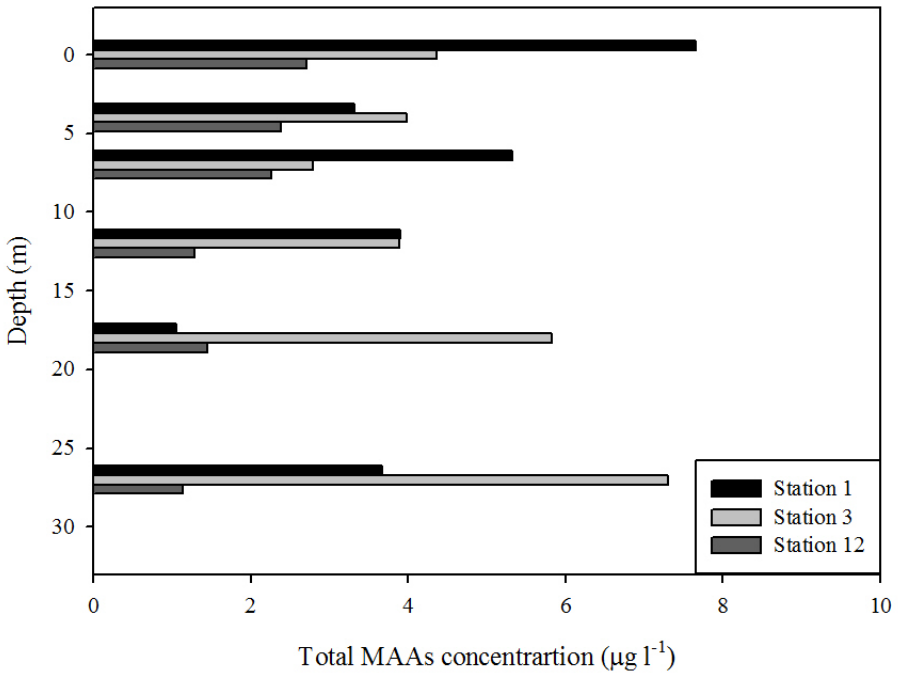

Figure 3.4.1. The depth distribution of total MAAs concentration in the western Arctic Ocean.

b. Light intensity

The penetration of UV-B was presented with the range from 4.8 to 8 m. The UV-A and PAR transmission depths ranged from 9.6 to 12 m and from 18 to 26 m (fig. 3.4.2).

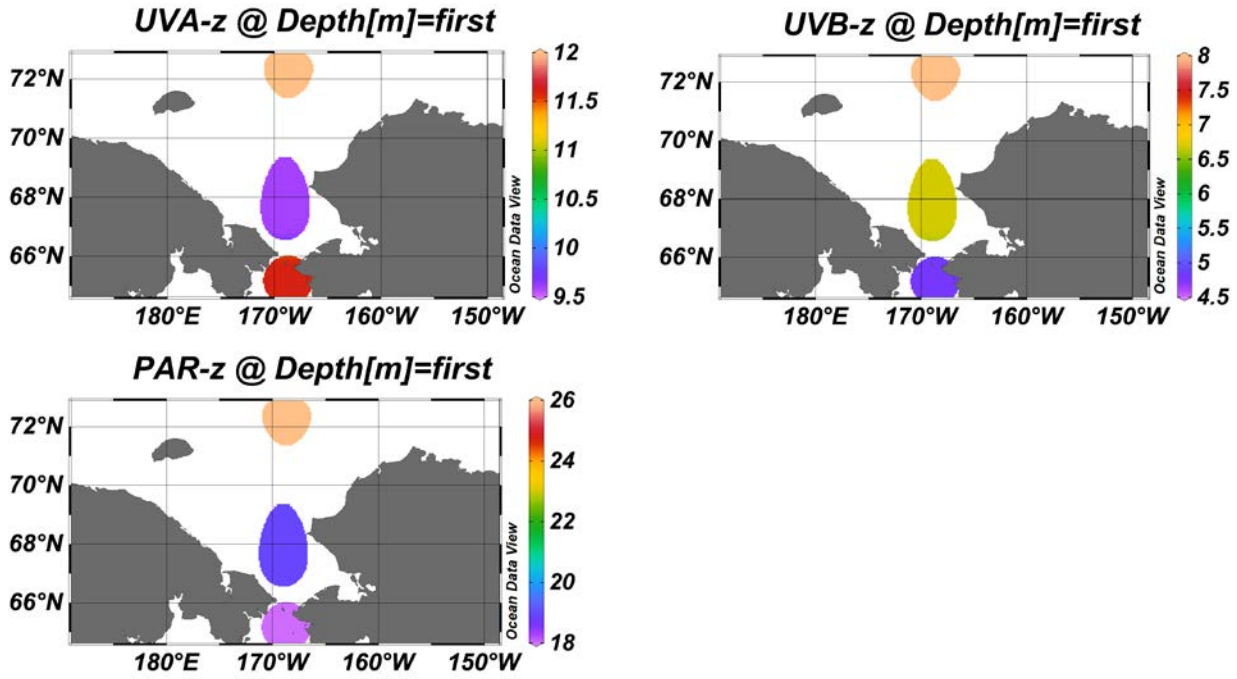

Figure 3.4.2. The penetration depth (Z: 1%) of PAR, UV-A, and UV-B in the western Arctic Ocean.

5) Estimation of Nitrogen source using CSIA-AAs

Bulk nitrogen stable isotope ratio of zooplankton is affected by trophic position or background nitrogen stable isotope ratio in the study area. In this research, background nitrogen stable isotope ratio is calculated by equation 1 and 2 eliminating trophic enrichment information of zooplankton from bulk nitrogen stable isotope ratio.

Bulk nitrogen stable isotope ratio of zooplankton were 11.3‰ and 10.7‰ in each station 2 and 12. Although the bulk nitrogen isotope of station 2 was higher than station 12, trophic position, which is calculated by nitrogen isotope ratio of amino acids, of zooplankton in station 12 (2.8) was higher than trophic position of zooplankton in station 2 (2.4) (Equation 1).

$$TP_{AAs} = [(\delta^{15}N_{Glu} — \delta^{15}N_{Phe} — 3.4) / 7.6] + 1 \text{ (Eq 1, Chikaraishi et al., 2009) (Equation 1)}$$

$$\delta^{15}N_{Primary\ Producer} = \delta^{15}N_{Consumer} - (TP_{AAs} – 1) * 2.5 \text{ (Equation 2)}$$

Trophic position calculated by nitrogen isotope of amino acids using Eq 1 was substituted with bulk nitrogen isotope in Eq 2 for estimating background nitrogen isotope. Background nitrogen isotope was 6.9‰, 7.15‰ in each station 2 and 12. Difference of background nitrogen isotope between station 2 and 12 was not large, which mean nitrogen source is not quite different between each stations. (Fig. 3.5.1)

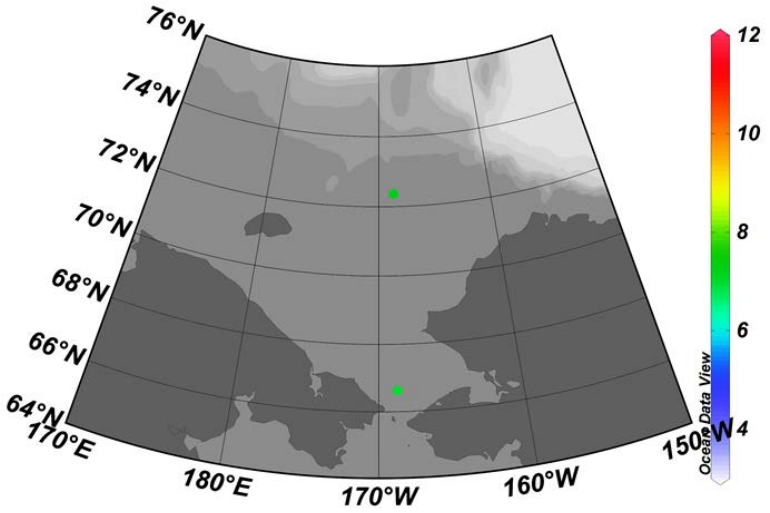

Figure 3.5.1. Background nitrogen stable isotope ratio in station 2 and 12 (‰)

Fraction of Meteoric water (MW), Pacific water (PW), Atlantic water (ATW) and Sea Ice Melt water (SIM) in the study area were calculated by salinity and oxygen stable isotope ratio for understanding water-mass source. (Table 3.5.1, Equation 3)

	Salinity (psu)	$\delta^{18}O$ (‰)
Atlantic Water (f_{AW})	34.87	0.24
Pacific Water (f_{PW})	32.5	-0.8
Meteoric Water (f_{MW})	0	-20
Sea Ice Melt water (f_{SIM})	4	-2

Table 3.5.1. Salinity and oxygen stable isotope ratio of each water-masses

$$f_{SE} + f_{SIM} + f_{MW} = 1$$

$$f_{SE}S_{SE} + f_{SIM}S_{SIM} + f_{MW}S_{MW} = S_{Observed}$$

$$f_{SE}\delta^{18}O_{SE} + f_{SIM}\delta^{18}O_{SIM} + f_{MW}\delta^{18}O_{MW} = \delta^{18}O_{Observed}$$

Equation 2. Calculation of water-mass fraction using salinity and oxygen stable isotope ratio

(f: fraction of water-mass, S: salinity, δ18O: oxygen stable isotope ratio of water-mass, SE: Saline Endmember (calculated by N:P ratio of the Pacific and Atlantic water), SIM: Sea Ice Melt water, MW: Meteoric Water)

Water-mass composition is slightly different along depth, SIM and MW fraction were 1~4% and 1~7%, while PW fraction was more than 80% at all stations.

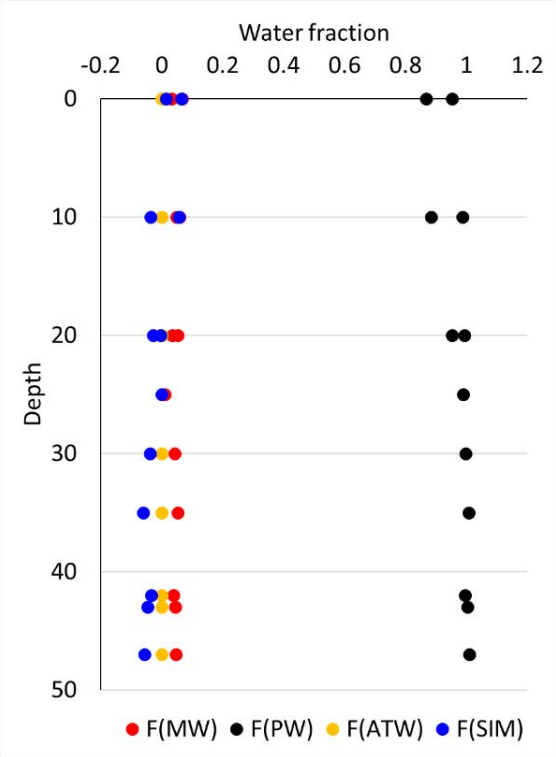

Figure 3.5.2. Water-mass fraction in station 1, 3 and 12

6) Air-sea CO_2 exchange and water column carbonate system: Carbonate system and its control factors in the Chukchi Sea in perspective of the changing arctic environment

The Arctic Ocean lies in the center of the current climate change as the summer sea-ice extent shrinks dramatically in recent years. Several modeling studies predict complete disappearance of the sea-ice extent in summer this century. One of the concerns resulting from this rapid change in the Arctic climate is the impact on the marine ecosystem in which carbon is the backbone of the energy flow initiated by solar energy. In addition, the shift of the ice-covered to the complete open ocean may lead to the change in the CO_2 flux across the sea-surface due to the imbalance in pCO_2 (Figure 3.6.1) between, which is ultimately driven by the primary production in the surface mixed layer and by the Arctic circulation. To investigate the change in the air-sea CO_2 flux (Figure 3.6.2) and the carbonate system interior of the water column, we have visited for 5 years the Chukchi Sea every summer season since 2010 and the Beaufort Sea in 2013 and 2014 onboard the Korean ice breaking R/V Araon. The areas surveyed were always undersaturated with respect to the atmospheric CO_2 despite large variability of the degree of saturation. We explored the spatial and temporal characteristics of the carbonate system in conjunction with the extent to which physical and biological properties would influence. To identify the driving forces in changing carbonate system interior of the water column, we focused on the impact of sea-ice melting, freshwater input from the continent, enhanced biological uptake driven by primary production, and chemical processes, which allow us to delve carbon flow in these particular area. In the presentation we will

discuss the results from the 5-year observations in the picture of the rapid change in the Arctic environment.

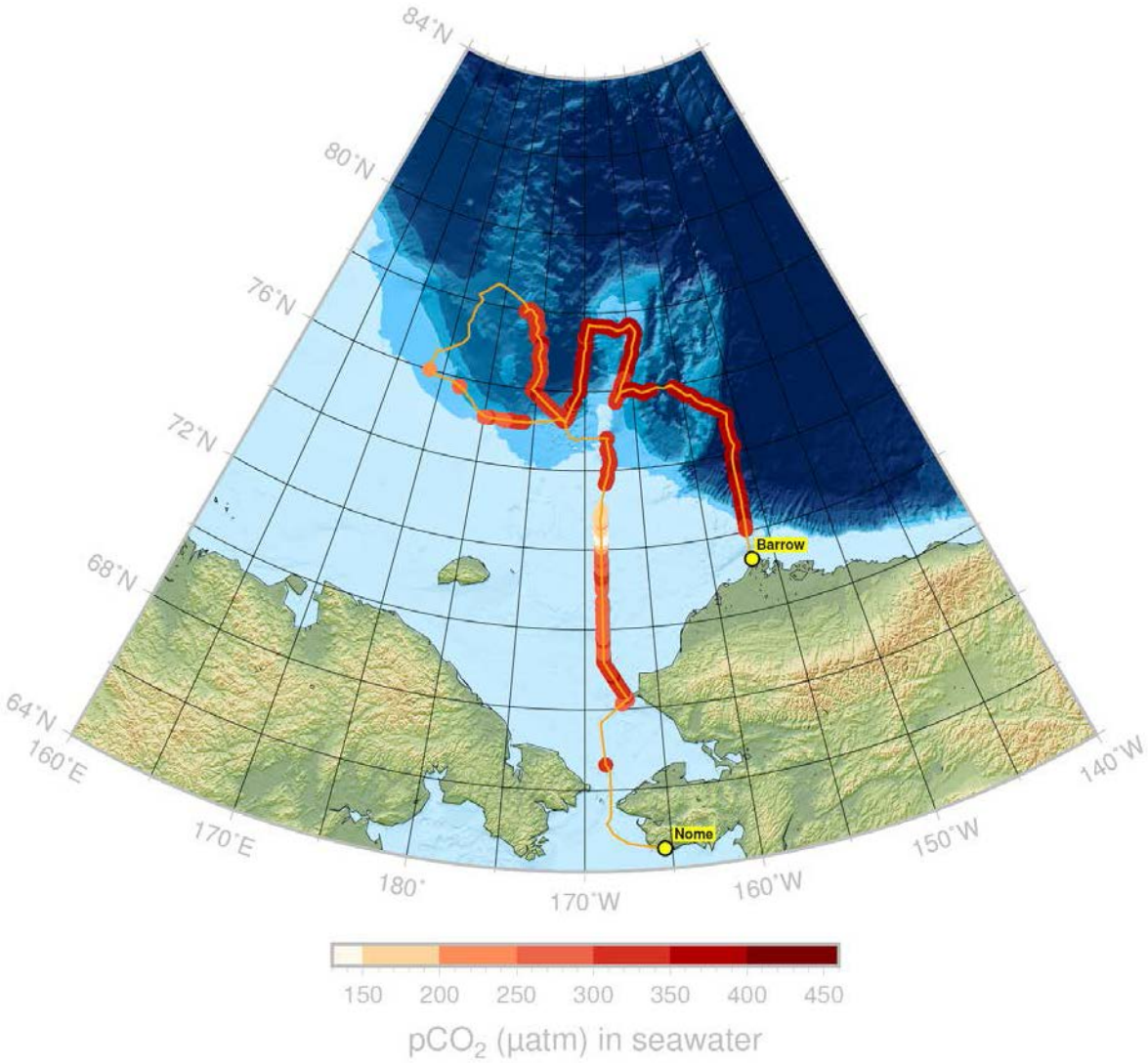

Figure 3.6.1. Spatial distribution of pCO_2 during 2016 Arctic cruise

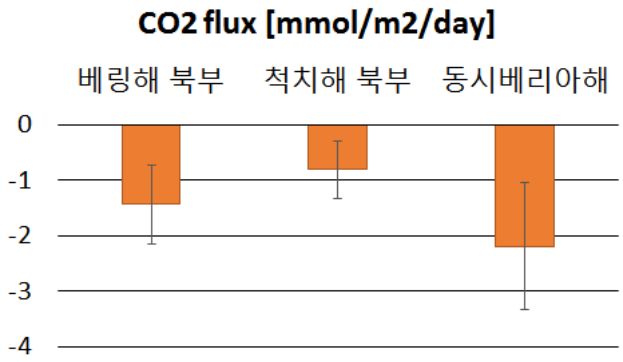

Figure 3.6.2. CO_2 flux in the Arctic Ocean

7) Microbial Oceanography

In August 2016, prokaryotic (i.e. Bacteria and Archaea) and viral abundances were determined at stations 1, 3, 10 and 12 within US EEZ waters. To analyze the microbial communities, seawaters (1-2 L) were sampled through 3.0 μm and 0.2 μm pore-sized Nuclepore filters (Whatman). Prokaryotic and viral abundances were measured using epifluorescence microscopy according to Noble and Fuhrman (1998). The Prokaryotic and viral abundances ranged from 7.2 to 28.0×10^5 cells ml^{-1} and from 8.6 to 22.2×10^6 cells ml^{-1}, respectively. Prokaryotic abundance was the highest at the surface of station 1, but the lowest at the surface of station 10. Viral abundance was the highest at the 25 m of depth at station 3, but the lowest at the 20 m of depth at station 1 (Fig. 3.7.1). The environmental DNAs of microbes are preserved at a laboratory in KOPRI.

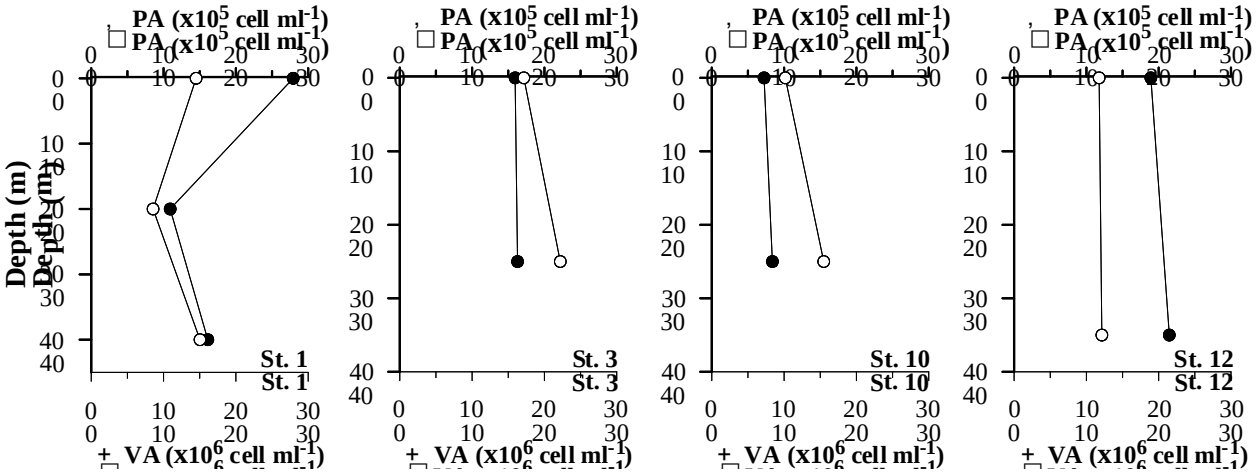

Figure 3.7.1. Distribution of prokaryotic (PA) and viral abundances (VA)

8) Chlorophyll-a concentrations and photosynthetic pigments

The photosynthetic pigments and chlorophyll-a concentrations were determined in the US EEZ

waters during August 2016. A total of 12 stations were visited and water samples were collected at 4-6 depths at each station including subsurface chlorophyll-a maximum layer.

The chlorophyll-a concentration varied from 0.10 to 6.66 μg/L with an average of 1.32 μg /L in this region (Fig. 3.8.1). The depth-averaged chlorophyll-a concentration was the highest at station 3 and the lowest at station 7. The micro- (>20μm) and pico- (<2μm) size chlorophyll-a concentrations made the highest and lowest contribution to total chlorophyll-a content, respectively 57.8% and 19.4% on average, indicating the large contribution of micro- and nano-size phytoplankton to primary production in this region. The subsurface chlorophyll-a maximum layer became developed between 10 to 50m depth.

The detected photosynthetic pigments of phytoplankton were chlorophyll-a, -b, -c2, -c3, fucoxanthin, alloxanthin, 19'-butanoyloxyfucoxanthin, prasinoxanthin, violaxanthin, 19'-hexanoyloxyfucoxanthin, diadinoxanthin, diatoxanthin, zeaxanthin, ββ-carotene, and the degradation products of chlorophyll.

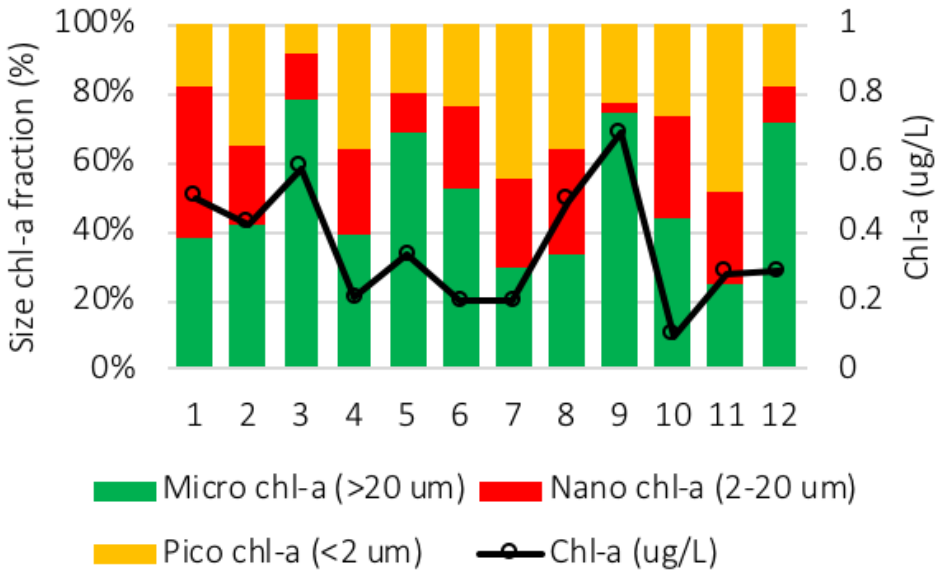

Figure 3.8.1. The surface chlorophyll-a concentrations (μgL^{-1}) and size-fractionated chlorophyll-a fractions (%) in August 2016.

9) Phytoplankton communities composition

Based on the HPMA slide method and SEM analysis, the samples were made for identifying species compositions of phytoplankton later at the laboratory in KOPRI (Fig. 3.9.1)

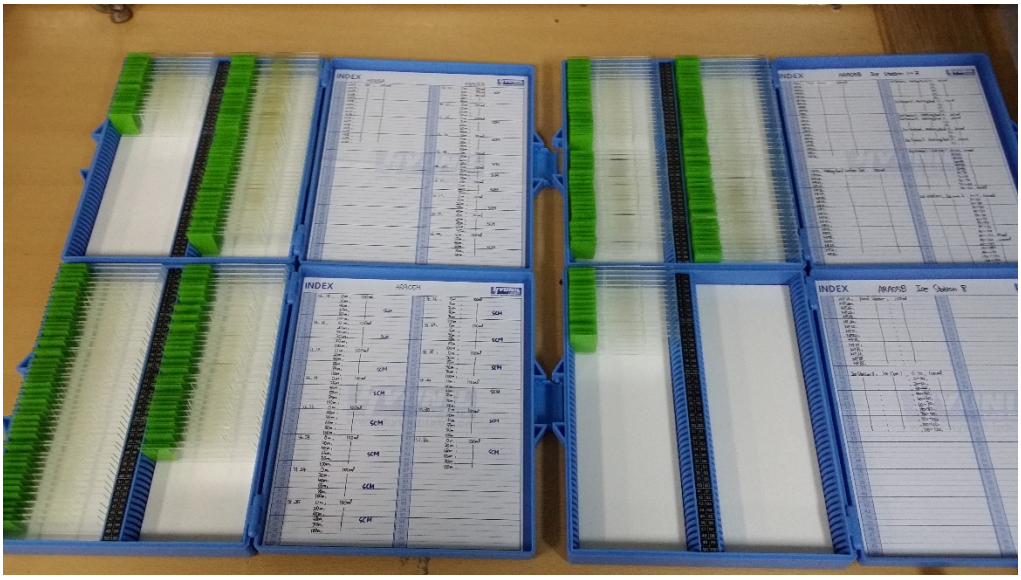

Figure. 3.9.1 HPMA Slides for Quantity analysis of phytoplankton communities.

10) Primary production and macromolecular composition

a. Primary production and new production

To investigate the spatial distribution of the primary production and new production of phytoplankton, seawater samples were collected in the 6 light depths (100, 50, 30, 12, 5, 1%) at station 1, 3, 6, 12. Then, the carbon uptake rates and the nitrate uptake rates were measured by using dual stable isotope tracers (^{13}C, $^{15}NO_3$).

The integrated carbon uptake rates of phytoplankton in euphotic layer ranged from 2.26 mg C m^{-2} h^{-1} to 54.12 mg C m^{-2} h^{-1}. The integrated nitrate uptake rates ranged from 0.18 mg N m^{-2} h^{-1} to 6.17 mg N m^{-2} h^{-1}. The highest carbon uptake rate was observed in the station 6 and the lowest carbon uptake rate was observed in the station 12 (Fig. 3.10.1). The highest and the lowest nitrate uptake rates also were observed in the station 6 and 12, respectively (Fig. 3.10.2). The carbon uptake rates of phytoplankton in the euphotic layer generally decreased with increasing depth except station 6 (Fig. 3.10.3). The nitrate uptake rates of phytoplankton in the euphotic layer also showed a similar vertical distribution (Fig. 3.10.4).

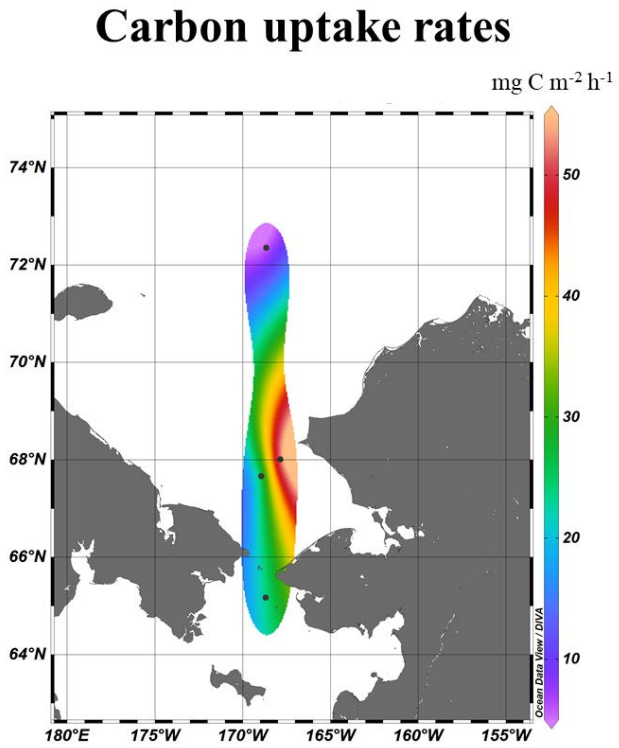

Figure 3.10.1. Spatial distribution of the carbon uptake rates of phytoplankton integrated in the euphotic layer.

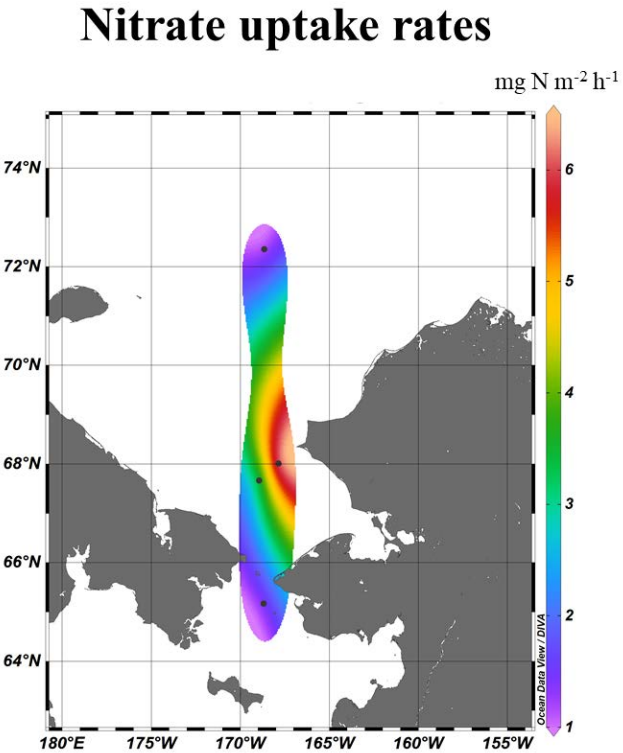

Figure 3.10.2. Spatial distribution of the nitrate uptake rates of phytoplankton integrated in the euphotic layer.

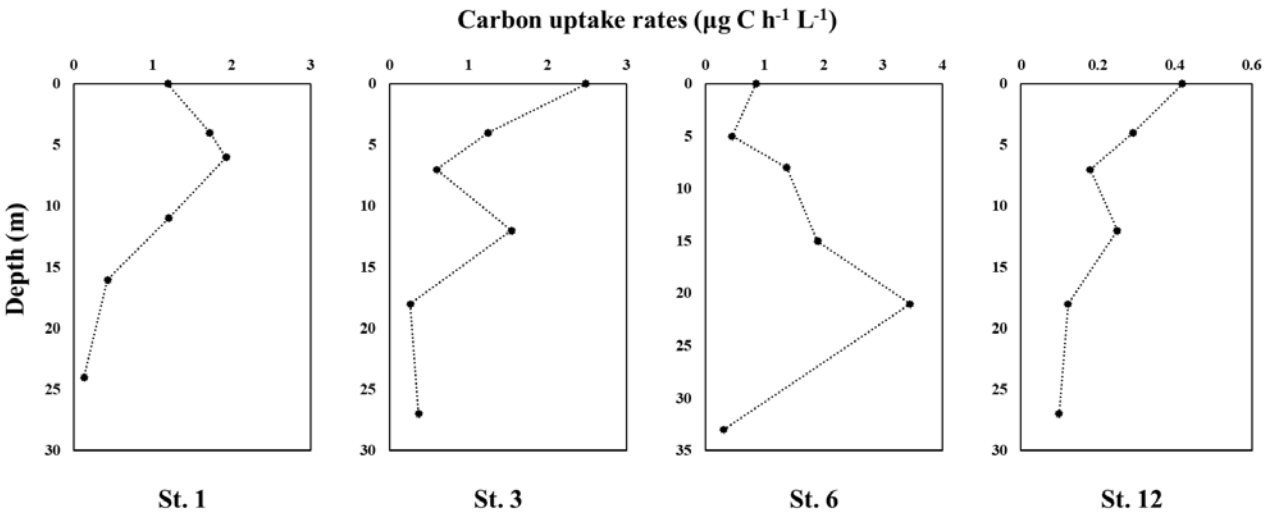

Figure 3.10.3. Vertical distribution of the carbon uptake rates of phytoplankton

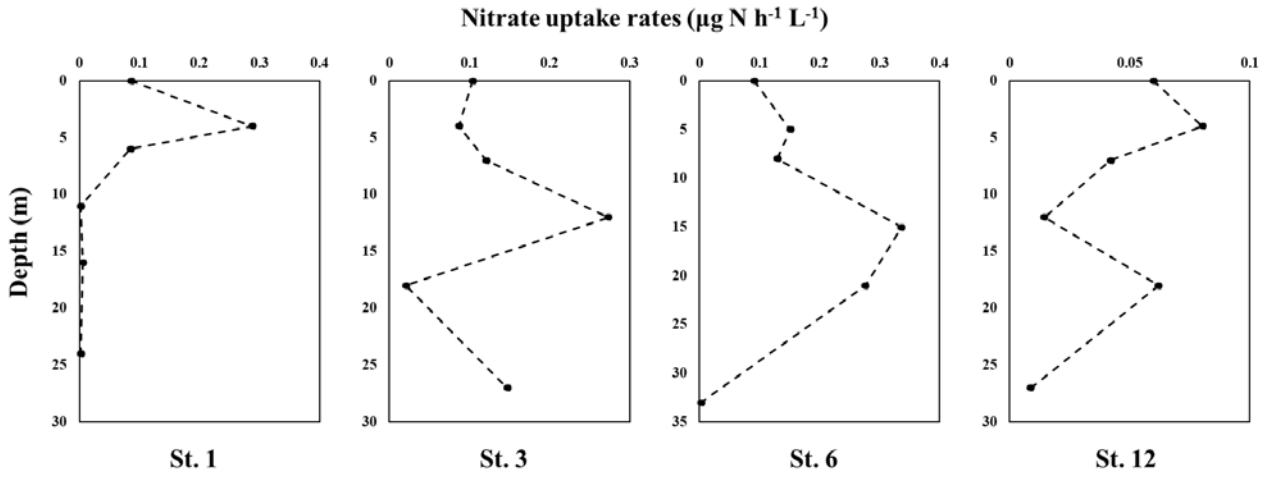

Figure 3.10.4. Vertical distribution of the nitrate uptake rates of phytoplankton.

b. Phytoplankton macromolecular composition

Phytoplankton consist of important biochemical components such as proteins, carbohydrates, and lipids. The proteins play a role in biological processes such as enzymatic catalysis and growth, and transfer carbon to herbivore biomass with higher efficiency than other biomolecular classes (Stryer,1988; Lindqvist and Lignell,1997). The lipids and carbohydrates act as an energy storage and are essential components of all membranes (Handa,1969; Parrish,1987). These biochemical components are known to be sensitive to environmental factors such as water temperature, salinity, nutrient concentration, and light conditions. Therefore, it is possible to obtain important information on the physiological state of phytoplankton and understand the current environmental condition through the study of macromolecular composition of phytoplankton. Thus, it is necessary to study the macromolecular composition of phytoplankton to understand how the current environmental

changes affect the arctic marine ecosystem.

The macromolecular compositions of phytoplankton were different at the 100%, 30%, and 1% light depths (Fig. 3.10.5). The percentage of carbohydrates in the EEZ ranged from 35% to 64%. Protein ranged from 15% to 33% and lipid ranged from 20% to 39%. Carbohydrates, proteins, and lipids in the euphotic zone decreased with increasing latitude (Fig. 3.10.6; 3.10.7; 3.10.8).

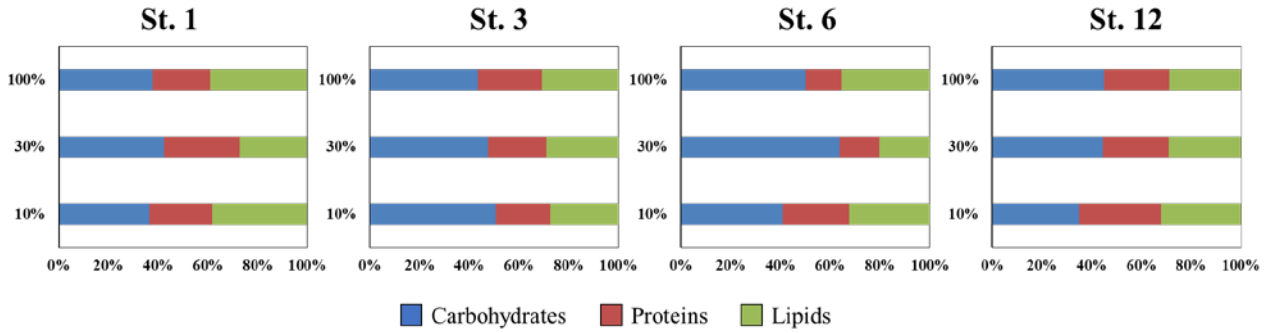

Figure 3.10.5. Biochemical compositions of phytoplankton in euphotic layer.

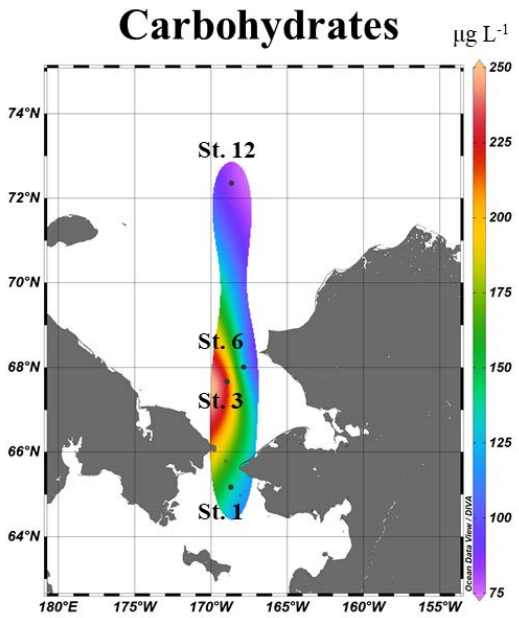

Figure 3.10.6. Mean concentrations of carbohydrates of phytoplankton in the euphotic layer

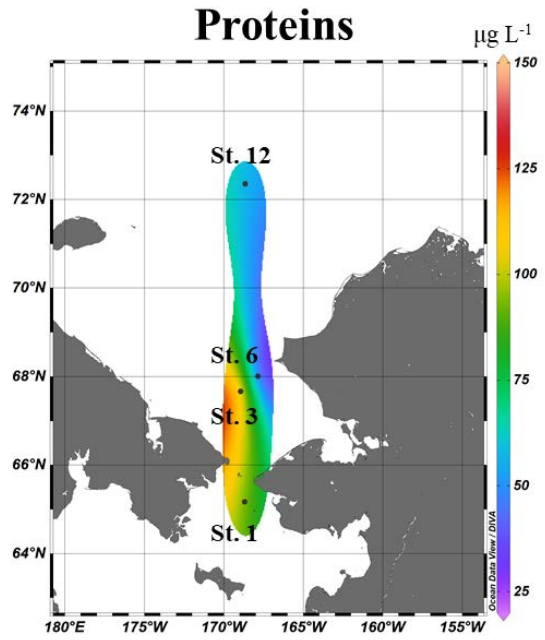

Figure 3.10.7. Mean concentrations of proteins of phytoplankton in the euphotic layer

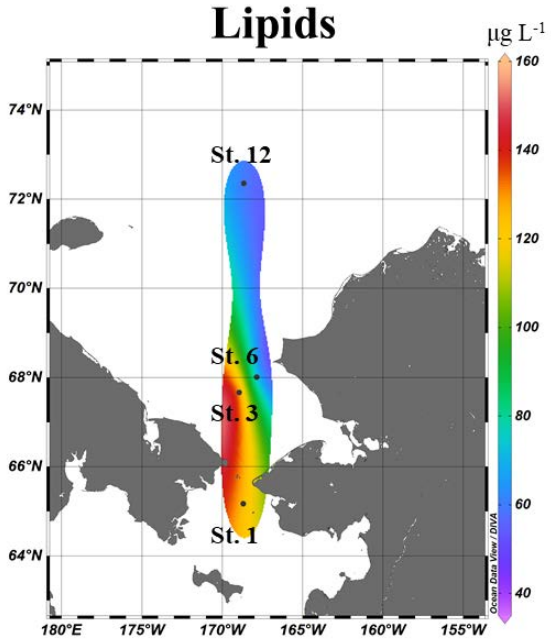

Figure 3.10.8. Mean concentrations of lipids of phytoplankton in the euphotic layer

11) Protozoa abundance and grazing rates on phytoplankton

Heterotrophic protozoa ingest a broad size spectrum of prey, from bacteria to phytoplankton, and are themselves important prey items for mesozooplankton. Many researchers suggest that heterotrophic protist contribute to the trophic linkage between phytoplankton and mesozooplankton and are important in the pelagic food webs of many oceanic waters. The importance of

heterotrophic protist in pelagic ecosystems has become increasingly evident in the past two decades, and trophic interaction between heterotrophic protists and phytoplankton has been reported in various marine. However, there is no information on the relative importance of heterotrophic protist in the pelagic ecosystem of the Western Arctic Sea. The Arctic Ocean is currently experiencing rapid environmental change due to natural and anthropogenic factor that includes warming, sea ice loss and other physical change as well as biology and ecosystem structure change. During this cruise, we investigated the meso-scale variations and structure of heterotrophic protozoan abundance and grazing rates on phytoplankton in the northern Bering Sea. In this study area, abundance of heterotrophic protozoa varied from 590 to 17,000 cells L^{-1}, and ciliates and heterotrophic dinoflagellate were dominant in heterotrophic protozoan group. Also, protozoan grazing rate on phytoplankton removed from 41 to 87% of daily primary production.

12) Mesozooplankton abundance and composition

Copepods constitute >70% of the total mesozooplankton biomass in Arctic waters, where they play a major role in energy flow and biogeochemical cycles. Some of the ingested organic carbon of zooplankton is used for metabolic activities, so quantifying this carbon is of prime importance to better understand energy transfer and elemental cycling via zooplankton in Arctic ecosystems. The Chukchi Sea is one of the major gateways into the Arctic where large quantities of Pacific heat, nutrients, phytoplankton and mesozooplankton enter the region through the shallow Bering Strait in a complicated mixture of water masses. Mesozooplankton abundance and biomass generally have been considered to be low in the Arctic Ocean. Nevertheless, mesozooplankton is numerically important element and plays a major role in the food webs. Mesozooplankton grazing, especially copepods, is a key factor controlling composition and dynamics of phytoplankton communities. In the Arctic Ocean, *Calanus* spp. are regarded as biological indicators of Arctic (*Calanus glacialis* and *C. hyperboreus*) and Atlantic (*C. finmarchicus*) water masses, respectively. They are the most important biomass species and the prime herbivores in these waters. Over the past several decades, atmospheric warming has increased the Arctic Ocean temperature and resulted in decreased extent and thickness of se ice. The removal of seasonal and permanent sea ice can greatly influence a number of important ecological processes such as photochemical reactions, stratification-related nutrient supply, phytoplankton bloom patterns and mesozooplankton distribution. For predicting climate change impacts in the ecosystems by rapid sea ice melting, it is important to understand the dynamics of the mesozooplankton community. The primary objectives were to understand the interactions between the environmental factors (i.e. seawater temperature, salinity and chlorophyll a concentration) and the mesozooplankton community. In this study area, zooplankton abundance varied from 9 to 827 indiv. m^{-3}, and zooplankton group were dominated by *Calanus glacialis* and Copepodite

13) Phytoplankton physiology (photochemistry)

Figure 3.13.1 shows the station map and the average maximal fluorescence (Fm), quantum efficiency of PSII (Fv/Fm) and functional absorption cross section (σPSII) in the mixed layer. The maximal fluorescence parameter indirectly indicates the biomass of phytoplankton. The values of Fm were higher in the Bering Strait than in the southern Chukchi Sea. This means that phytoplankton biomass was significantly different in the two regions. The values of Fv/Fm were higher than 0.5 at all stations and there was no regional difference in the Fv/Fm. This indicates that the nutrient limitation for phytoplankton photosynthesis is low in the surface layer. The values of σPSII represented (500–600) x 10-20 m^2 $photon^{-1}$ at all station but more than 600 x 10-20 m^2 $photon^{-1}$ at station 3. The large values of σPSII may be due to the size of phytoplankton community. It needs to compare with phytoplankton community data.

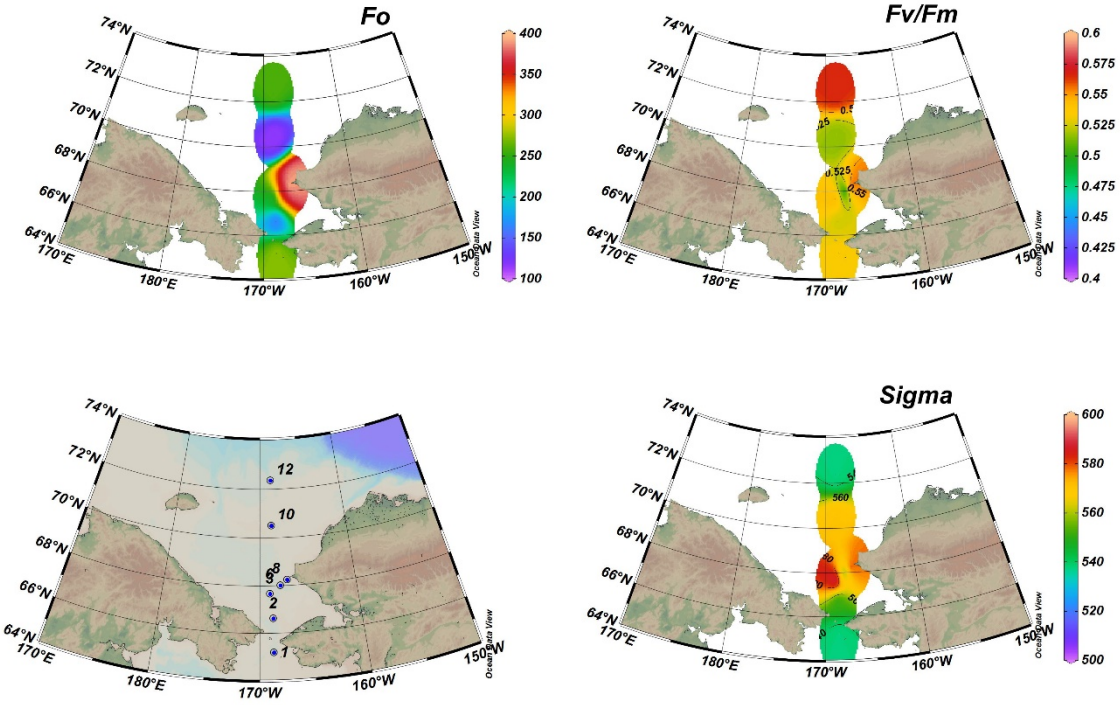

Figure 3.13.1. Station map and the spatial distribution of minimal fluorescence (Fo), quantum efficiency of PSII (Fv/Fm) and functional absorption cross section (σPSII).

The above three fluorescence variables are shown as vertical distribution (Fig. 3.13.2). The values of Fo were high in the surface layer from station 1 to station 8, and were high at the depth of 20-30 m from station 10. This represented that the vertical distribution of phytoplankton was different between the Bering Strait and the southern Chukchi Sea. On the other hand, Fv/Fm was similar at all depths. The σPSII values were relatively high at station 3 and very low at station 1. As

with the surface layer, it is necessary to compare it with phytoplankton community data at all depths. Overall phytoplankton biomass and vertical distribution were distinctly different, but Fv/Fm was similar between the Bering Strait and the southern Chukchi Sea. Phytoplankton community data will be compared with the fluorescence variables at each station.

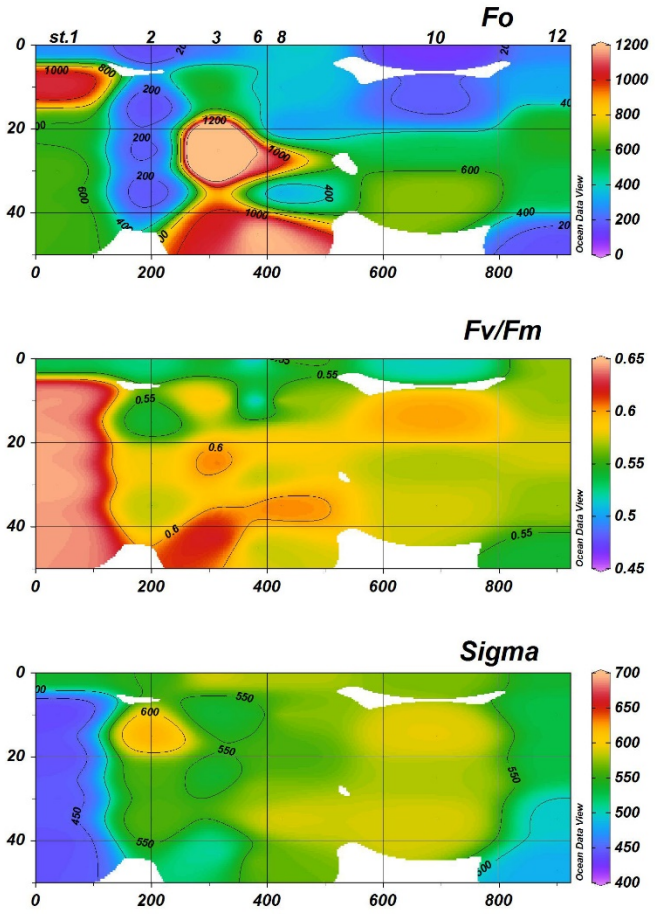

Figure 3.13.2. The vertical distribution of minimal fluorescence (Fo), quantum efficiency of PSII (Fv/Fm) and functional absorption cross section (σPSII).

14) Ocean Optical Observation

The results from the IOPs will be able to show the bio-optical characteristics in water at each station and at each depth of the water sample (Fig. 3.14.1).

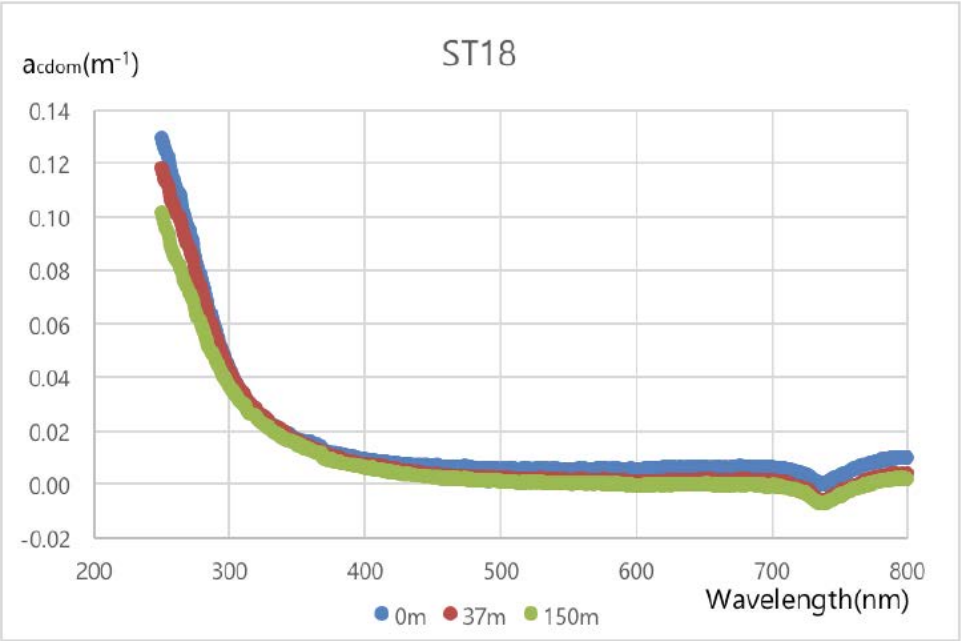

Figure 3.14.1. An example of absorption colored dissolved organic matter at the station 18.

During this Arctic cruise, data for calibration/validation of satellite remote sensing ocean color data were collected. The IOPs reflected the bio-optical characteristics in water at the selected depths. The results from the AOPs, i.e. data from HPRO II and TriOS, reflect the continuous bio-optical characteristics of water surface and the bio-optical profiles at the operated station (Fig. 3.14.2). We are going to use these field data for further detailed examination and correction of satellite data.

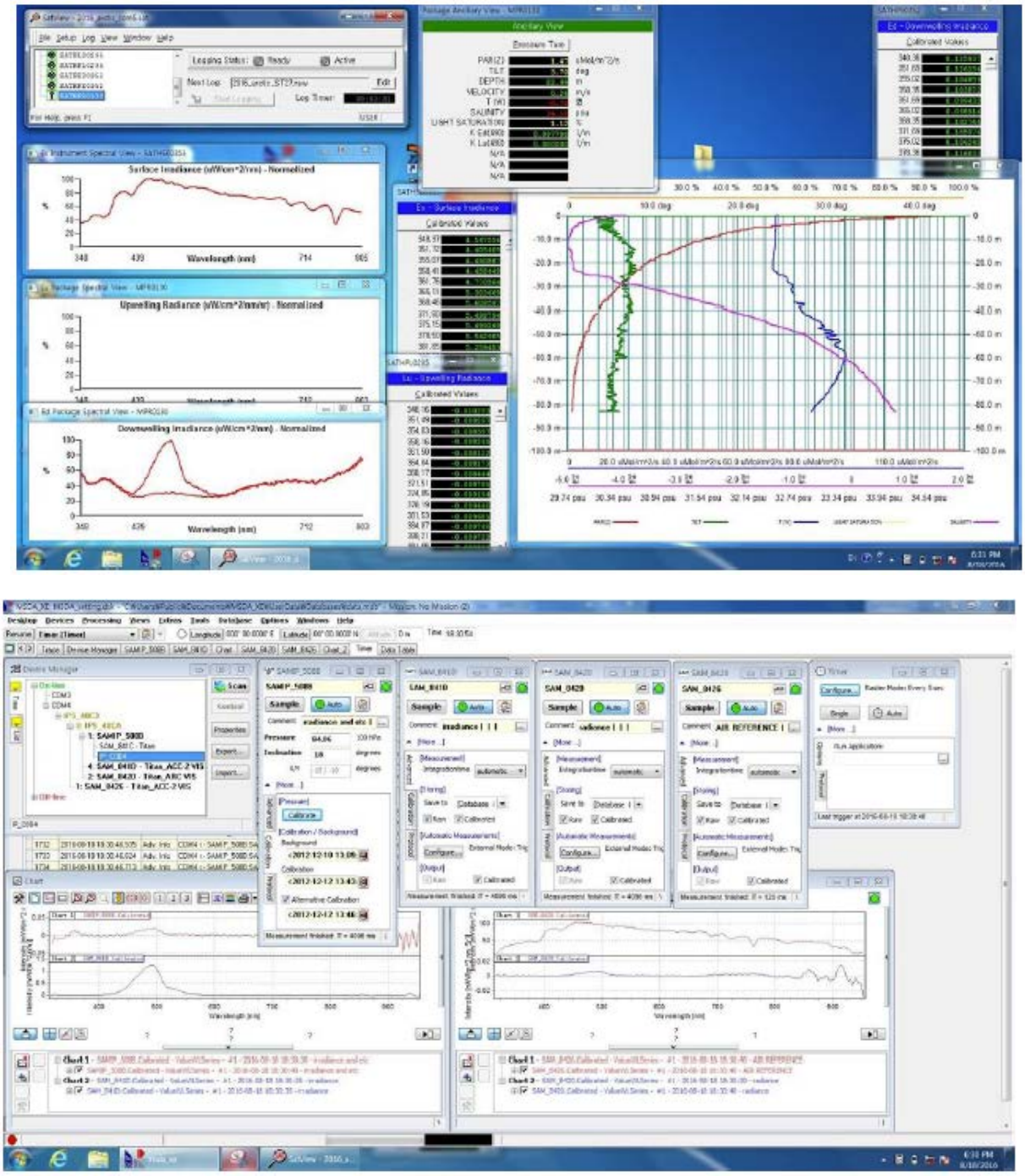

Figure 3.14.2. An example of HPRO II (up) and TriOS (down) data signal recorded at the station 28.

15) Atmospheric Observations

Figure 3.15.1 shows the air pressure records measured by PTB110 at the foremast and the air temperature and relative humidity records measured by HMP155. On the second day of cruise (August 6), the ship entered the Arctic Circle (66°N). From the fourth day (August 8) the air temperature dropped quickly below the freezing level while the vessel voyaged northeastward

through the Chukchi Sea. On August 9-10, the air temperature dropped below freezing level (minimum -5 °C) while the pressure increased (maximum around 1020 hPa). The relative humidity at departure was around 50-60% and increased sharply to around and over 90% after the second day of cruise.

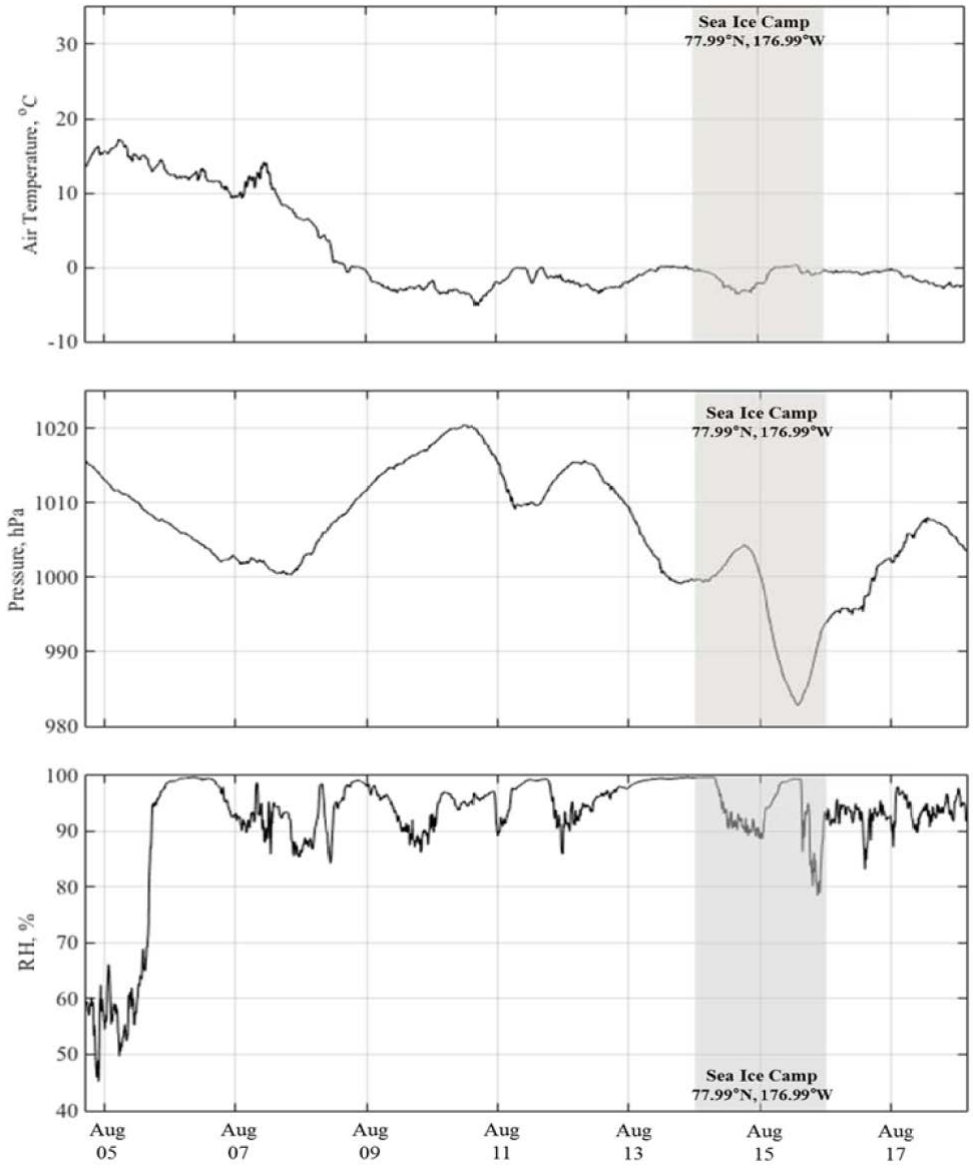

Figure 3.15.1. (Top) Air temperature (degC) : HMP155 at the foremast. (Middle) Pressure (hPa) : PTB110 at the foremast. (Bottom) Relative humidity (%) : HMP155 at the foremast.

Figure 3.15.2 shows the calculated true wind speed and direction considering the head, course, and speed of the ship. While voyaging in the EEZ (before August 9), the wind directions changed from easterlies to northeasterlies and the wind speeds were mild below 10 m/s maximum.

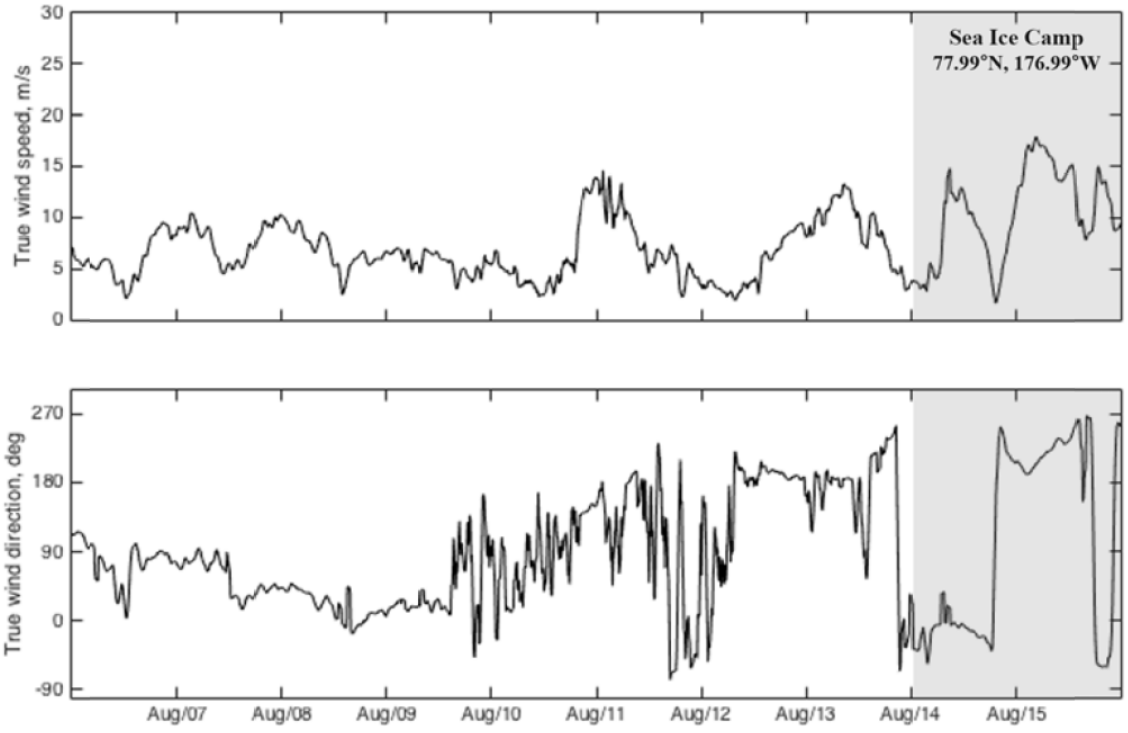

Figure 3.15.2. (Top) 10-min averaged true wind speed (m/s) and (Bottom) direction (deg).

Figure 3.15.3 displays the time series of downwelling shortwave (DSR) and longwave radiations (DLR) measured by the CNR4 net radiometer at the foremast. The DSR shows an apparent diurnal cycle associated with the diurnal variation of solar zenith angle. The sunny day peak value almost reached 700 W m^{-2} on 00 UTC August 5 around the latitude of 64°N. However, it dropped a lot by 230 W m^{-2} next day when the sky was overcast. The amplitude of the DLR was also an indication of the existence of clouds and fogs. In the sunny day on August 5, it was around 300 W m^{-2}, while increased to almost 400 W m^{-2} next overcast day (August 6).

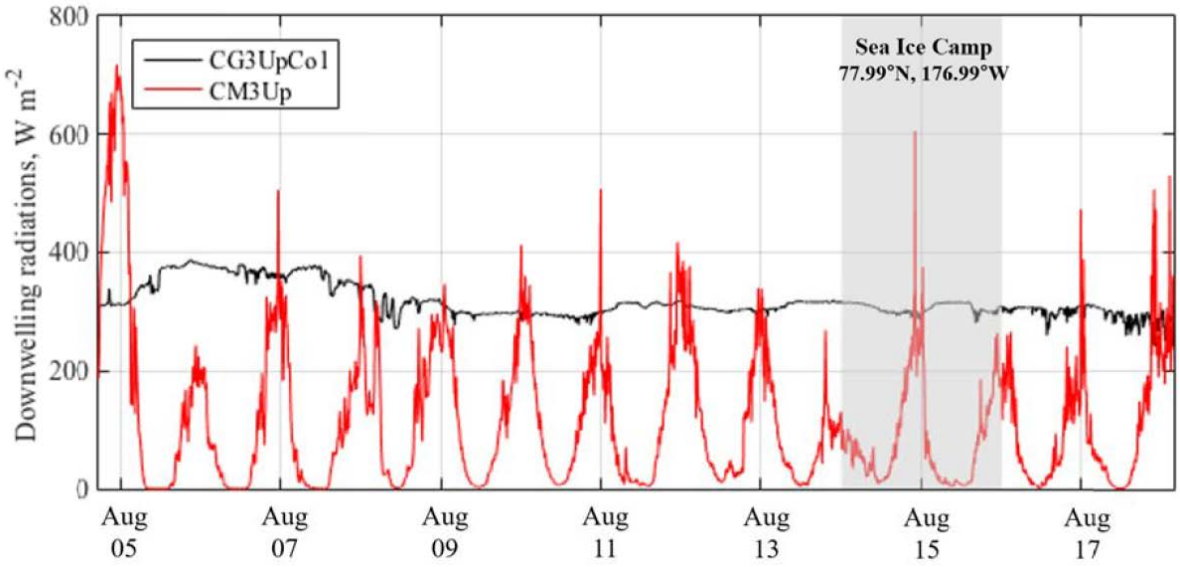

Figure 3.15.3. Downwelling radiations [W m^{-2}]: (black) longwave radiation, (red) shortwave radiation. Positive sign denotes downward direction.

4. Publications

Guangjian Xu, EunJin Yang, Yong Jiang, Kyung-Ho Cho, Jinyoung Jung, Youngju Lee,Sung-Ho Kang, Can pelagic ciliates indicate vertical variation in the water quality status of western Arctic pelagic ecosystems?, Marine Pollution Bulletine, 2018, 133, 182-190